2012

Electrical conduction in chalcogenide glasses of phase change memory

Marco Nardone
Bowling Green State University, marcon@bgsu.edu

M. Simon

I. V. Karpov

V. G. Karpov

Electrical conduction in chalcogenide glasses of phase change memory

M. Nardone, M. Simon, I. V. Karpov, and V. G. Karpov

Citation: Journal of Applied Physics **112**, 071101 (2012); doi: 10.1063/1.4738746
View online: http://dx.doi.org/10.1063/1.4738746
View Table of Contents: http://scitation.aip.org/content/aip/journal/jap/112/7?ver=pdfcov
Published by the AIP Publishing

APPLIED PHYSICS REVIEWS—FOCUSED REVIEW

Electrical conduction in chalcogenide glasses of phase change memory

M. Nardone,[1,a)] M. Simon,[2] I. V. Karpov,[3] and V. G. Karpov[2]
[1]*Department of Environment and Sustainability, Bowling Green State University, Bowling Green, Ohio 43403, USA*
[2]*Department of Physics and Astronomy, University of Toledo, Toledo, Ohio 43606, USA*
[3]*Intel Corporation, SC9-09, 2200 Mission College Blvd., Santa Clara, California 95052, USA*

(Received 25 March 2012; accepted 30 May 2012; published online 1 October 2012)

Amorphous chalcogenides have been extensively studied over the last half century due to their application in rewritable optical data storage and in non-volatile phase change memory devices. Yet, the nature of the observed non-ohmic conduction in these glasses is still under debate. In this review, we consolidate and expand the current state of knowledge related to dc conduction in these materials. An overview of the pertinent experimental data is followed by a review of the physics of localized states that are peculiar to chalcogenide glasses. We then describe and evaluate twelve relevant transport mechanisms with conductivities that depend exponentially on the electric field. The discussed mechanisms include various forms of Poole-Frenkel ionization, Schottky emission, hopping conduction, field-induced delocalization of tail states, space-charge-limited current, field emission, percolation band conduction, and transport through crystalline inclusions. Most of the candidates provide more or less satisfactory fits of the observed non-linear IV data. Our analysis calls upon additional studies that would enable one to discriminate between the various alternative models. © *2012 American Institute of Physics*. [http://dx.doi.org/10.1063/1.4738746]

TABLE OF CONTENTS

a)Electronic mail: marcon@bgsu.edu.

I. INTRODUCTION

Chalcogenide materials have recently regained strong interest due to their ability to repeatedly transform between glassy (disordered) and crystalline (ordered) atomic structures. One application is the storage of digital data where 1s and 0s are recorded as either glassy (high resistive and low-reflective) or crystalline (low resistive and high reflective) structures. For example, optical memory disks use laser light to convert small portions of a thin chalcogenide film between the high and low reflective states. On the other hand, phase change memory (PCM) uses a voltage bias to convert the material between the high and low resistive states. PCM stores data in a smaller area and with higher speeds for both read and write processes than the optical memory disks.

PCM is an emerging nonvolatile memory technology with the capability of random access memory, it is sometimes referred as unified memory. Applications explored for this technology span from wireless, embedded systems[1] to solid state storage,[2] automotive,[3] and space applications.[4] Most recently, usage of PCM in computer applications was suggested as storage class memory (SCM).[5]

Large, up to 1 gigabyte, memory arrays with PCM elements have been demonstrated for 180 nm,[6] 90 nm,[7,8] and 45 nm (Ref. 9) technology nodes. In PCM, each individual element is in series with an access/selector device. Both

MOS-based[6] and bipolar junction transistor/diode-based[8] selectors have been integrated with PCM. Recently, PCM was integrated with a chalcogenide based thin film selector to form arrays,[10] opening a path for 3D stackable cross point phase change memory.[11]

The operation of PCM depends on charge transport in their constituent inclusions of chalcogenide glasses. When the device is in the reset state, the electrical conduction can be non-ohmic under practical voltages and temperatures. This non-ohmicity provides a way of supplying energy to the device faster than ohmic conduction and it needs to be properly understood in order to improve future device parameters.

The goal of this focused review is to recall the established physics of chalcogenide glasses and convey a broad picture of different mechanisms that are relevant to the problem of non-ohmic conduction in these materials. Ultimately, we provide a starting point for the additional studies that are required to better understand charge transport in PCM glasses.

The commonly observed nonlinear current-voltage (IV) characteristics (above $\sim 10^3 - 10^4$ V/cm) are often attributed to the Poole-Frenkel (PF) effect after the classical work[13–15] suggesting their plausible interpretation. An experimental signature of PF conduction is a region of linearity in the plot of $\ln(I/I_0)$ vs. either $\sqrt{V}$ or V where I_0 is the pre-exponential factor. The underlying mechanism is commonly related to the field-induced increase in free carrier concentration, as reflected in Refs. 16–23 (except Ref. 24 which proposes hopping conduction).

Although there is general agreement about the observed PF-type of non-ohmicity and the fact that $I_0 \propto \exp(-E_a/kT)$, where E_a is the activation energy, k is the Boltzmann constant, and T is temperature, particular features observed and especially their interpretations vary dramatically between researchers. We note, for example, that Refs. 16–19 and 23 present their observed non-ohmicity as $\ln(I/I_0) \propto \sqrt{V}$, while Refs. 20, 22, and 24–28 describe their observations as $\ln(I/I_0) \propto V$. Furthermore, some of the latter results[25,28] point at two different domains in the IV data which exhibit different proportionality coefficients and temperature dependencies.

In this review, we frame what is known about dc conduction in chalcogenide glasses, indicate shortcomings in our current state of understanding, and suggest avenues for further investigation. We begin with a brief overview of the pertinent experimental data to provide some context for the key observations. That is followed by a review of the physics of localized states, which underlies the unique properties of chalcogenide glasses. Then we provide a survey of conduction mechanisms that may explain the observed non-ohmic IV data, including: (1) the original Poole-Frenkel mechanism; (2) Schottky decrease in interfacial barrier near device electrodes; (3) field-induced delocalization of shallow band tail states near the mobility edges; (4) space charge limited (injection) currents; and (5) field effects in hopping conduction. Here, we discuss these and some other possible mechanisms of dc conduction in chalcogenide glasses including bulk materials and thin films down to the nanometer scale. Finally, we provide a summary of the candidate mechanisms and discuss their validity and implications, along with new indicative facts that are required to further evaluate these mechanisms.

II. EXPERIMENTAL DATA: A BRIEF OVERVIEW

The interpretation of experimental data related to dc conduction in amorphous chalcogenides must consider fabrication technology, whether the sample is amorphous or vitreous in nature, cell geometry, and other factors. These materials have been intensely investigated over the past half century, but in this brief overview we present only some representative results for bulk and thin glassy chalcogenides with various compositions, including the typical composition of $Ge_2Sb_2Te_5$ (GST) for modern PCM devices.

Certain universal features can be cited for amorphous chalcogenides, including the thermally activated conductivity $\sigma \propto \exp(-E_a/kT)$, positive thermopower indicative of p-type conduction, and negative Hall coefficient.[12] In magnitude, the activation energy for conduction, E_a, is close to half the mobility gap and can range from 0.3 to 1 eV, with a typical value of $E_a \sim 0.37$ eV for modern PCM devices under low bias.[29] Hopping conductivity with its classic temperature dependence, $\sigma \propto \exp[(-T_0/T)^{1/4}]$, is generally not observed, with the exception[30] of some unannealed, sputtered films.

Historically,[31] the study of bulk chalcogenide glasses revealed dc conductivity described by $\sigma \propto \exp(F/F_0)$ for fields up to $F \sim 1 - 4 \times 10^5$ V/cm, above which there was a steep increase in the field dependence. Typically, there was also an ohmic region observed at fields below $10^3 - 10^4$ V/cm; that transition field was found to increase linearly with thickness.[28] In some cases, usually below room temperature, two distinct exponential regimes were observed: a lower field region with $\ln\sigma \propto (F/F_{01})$ followed by a steeper region with $\ln\sigma \propto (F/F_{02})$.[28,32,33] The slopes F_{01} and F_{02} had opposite temperature dependencies and F_{01} was independent of sample thickness while F_{02} increased linearly with thickness (indicative of space charge limited current, as discussed in Sec. IV D). Near and above room temperature, only the lesser slope F_{01} was observed and the conductivity and slope were found to be independent of thickness in the range[34] 10 μm to 1 mm and also in the range[33] of 0.2 to 1.1 μm.

The work in Ref. 24 investigated subthreshold dc conduction in modern GST PCM devices with thicknesses on the order of 100 nm and over a temperature range of 25 to 85 °C. Cell geometries included lance (vertical with "hemispherical" amorphous dome) and μtrench[35] configurations. An ohmic regime was observed in the IV data at applied voltages $V_a < 0.3$ V (or fields $F \lesssim 3 \times 10^4$ V/cm), followed by an apparent exponential dependence of $\ln I \propto V$. In the non-ohmic region, the activation energy was found to decrease linearly from 0.35 to 0.28 eV with increasing voltage. At yet higher voltages of 0.8 to 1 V, the slopes of the $\ln I$ vs. V curves were found to be inversely proportional to temperature. These IV characteristics and temperature dependencies were corroborated in Ref. 22 for 100 nm thick amorphous GST films (and other compositions).

In contrast to the above results, a recent study[23] of GST PCM lance devices in the reset state, with thicknesses of less than 50 nm, presented IV data that were best described by $\ln I \propto \sqrt{V}$. An ohmic region was not observed but we note, however, that for such thin devices a field of 10^4 V/cm

corresponds to an applied voltage of 0.05 V, below which data was not presented; hence, the low field region may not have been studied. Results of other work[17] for as-deposited amorphous GST films with thicknesses of 20 to 100 nm showed the same $\sqrt{V}$ dependence at fields of $F > 10^4$ V/cm and an ohmic regime for lower fields. The slope of the ln$I$ vs. $\sqrt{V}$ curves increased slightly with temperature in the range 295 to 323 K (opposite to the above discussed results in Ref. 24). The IV data in both Refs. 17 and 23 show a stronger field dependence near the threshold field.

A systematic investigation of thickness-dependent effects in thin glassy films was reported in Ref. 19. Low-field ohmic and a high-field non-ohmic ln$I$ vs. $\sqrt{F/F_0}$ regions were observed in IV data over a temperature range of 130 to 373 K and a thickness range of 130 to 600 nm for various compositions of GeBiSbS alloys. The measured current showed only a weak dependence on sample thickness and the slope, F_0, was thickness independent.

More recently,[36] a nonlinear relationship between low-field resistance and thickness was reported for μtrench GST PCM cells with amorphous GST thicknesses between 8 and 35 nm. However, the different thicknesses, which were obtained by varying the reset pulse, were calculated from the IV data by assuming the correctness of a modified Poole-Frenkel conduction mechanism.[37] The reported thickness dependencies do not account for the possible leakiness of such thin samples. That data are further discussed in Sec. V below.

In summary, as shown in Fig. 1, the experimental data suggest that there are three major field-dependent regimes: (1) an ohmic region at low field $F \lesssim 10^3 - 10^4$ V/cm (which can also be the start of a subsequent non-ohmic dependence); (2) an exponentially field-dependent regime (possibly two distinct relations depending on temperature and thickness), with ln$I \propto V$ or $\propto \sqrt{V}$ behavior, or some combination thereof; and (3) a stronger field dependence, possibly ln$I \propto V^2$, near the threshold field. The ohmic region may not be observed for very thin devices (e.g., thickness less than 100 nm), since the transition field is directly proportional to the thickness. There is evidence that the activation energy decreases linearly with increasing voltage in the intermediate field region. In general, the conductivity at or above room temperature appears to be nearly thickness independent, at least down to 100 nm.

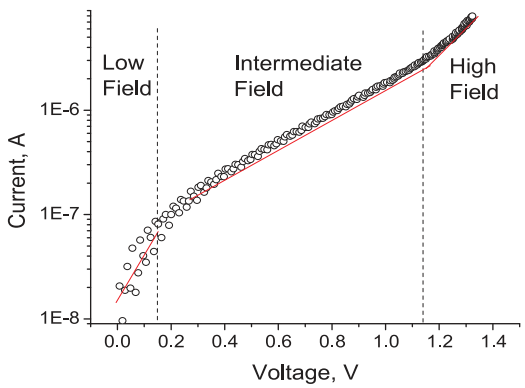

FIG. 1. Three regions in the IV characteristic of an unspecified chalcogenide PCM device that is representative of the results discussed in the experimental overview. The low-field region is usually described as ohmic, but in some cases of thin samples it is described as ln$I \propto V$. The intermediate region has exponential dependence described as either ln$I \propto V$ and/or $\propto \sqrt{V}$. Near and below room temperature, two slopes are often observed in the intermediate region. The high field region corresponds to a stronger dependence, possibly ln$I \propto V^2$.

III. ELECTRONIC STATES IN CHALCOGENIDE GLASSES

In this section, we recall the unique nature of charge transport in amorphous materials and the peculiar features of localized states in chalcogenide glasses. The electronic structure of disordered systems is inherently different than crystalline materials. The most important distinctive property of disordered materials is the short mean free path l that can be as small as the minimum quantum limit defined by $kl \gtrsim 1$, where k is the wavenumber. The strong scattering is due to intrinsic imperfections and random fluctuations of the potential energy.[12]

Since scattering in the disordered system is strong enough, $kl \sim 1$, the electronic wavefunction is effectively "localized" to exist within a span of its wavelength. The celebrated work[38] by Anderson in 1958 showed that random fluctuations in local site energies can create these localized states from which the wavefunctions fall off exponentially with distance. Although these states share many similarities with traps in crystalline materials, the unique feature is that in amorphous materials there can be continuous distributions of such states that remain localized even if neighboring wavefunctions overlap. As a result, with sufficient disorder all diffusive transport can cease (except for thermal activation) and the conductivity will tend to zero at the zero of temperature even if localized states exist at the Fermi energy. The possibility of thermal activation facilitates hopping diffusion via localized states. The corresponding hopping conduction can be efficient enough to dominate over the band transport in such materials as a-Si and a-Ge. However, it is significantly suppressed in chalcogenide glasses due to a very unique nature of their localized states as explained next.

Within a broader scope, deviations from structural periodicity smear out the sharp energy bands into smooth transitions between localized and non-localized states that are separated by a distinct energy level, referred to as the mobility edge.[12] Furthermore, a disorder and structural defects (such as dangling bonds) can lead to a continuous localized energy spectrum in the mobility gap and a finite density of states (DOS) at the Fermi energy (see Figs. 5 and 9). While that is true of any amorphous structure, the uniqueness of glassy semiconductors stems from the "softness" of the atomic lattice, wherein the local atomic configuration can change significantly depending on the occupation number of the localized state. Hence, one must consider the consequences of electron-lattice interactions due to strong polaron effects, which, in particular, can significantly suppress the hopping transport. A summary of the observed phenomena and corresponding theoretical explanations that are relevant to our discussion of conduction mechanisms are provided next.

A. Conflicting observations

Thorough reviews of experimental data related to electronic transitions in chalcogenide glasses can be found in Ref. 12, with more limited reviews given later in Refs. 40 and 41. Here we summarize some of the results that are pertinent to charge transport and the significance of localized electronic states.

Beyond the specific observations cited in Sec. II, experimental data on the various electronic properties of chalcogenide glasses can be broken into two groups, one of which testifies in favor of a high DOS in the mobility gap, while another states the opposite. To explain the data that suggests the high DOS, we consider the band diagrams shown in Fig. 2, which assume the standard one-electron localized states associated with all energy levels in the mobility gap. In the top left diagram, the localized states can provide efficient screening of an external electric field (shown as the tilted band edges) by redistributing the localized electrons in such a way as to form a screening dipole layer. The left bottom diagram illustrates another property of this system: strong electron spin resonance (ESR) associated with the states in the vicinity of the Fermi level occupied by single electrons whose spins can be aligned with the external magnetic field (electron states well beyond the Fermi level can be occupied by pairs of electrons with opposite spins that do not contribute to ESR). The dashed arrows in the top right diagram show the transitions corresponding to a considerable (proportional to the high density of localized electron states) optical absorption for the photon energies $\hbar\omega$ smaller than the mobility gap G. Finally, the bottom right diagram illustrates hopping conduction via localized states close to the Fermi level. All the above phenomena—strong screening and ESR, noticeable absorption at $\hbar\omega < G$, and hopping—are observed in the tetrahedral amorphous semiconductors a-Si and a-Ge, for which the model of a high DOS of one-electron localized states in the mobility gap then appears fully adequate and comfortably self-consistent.

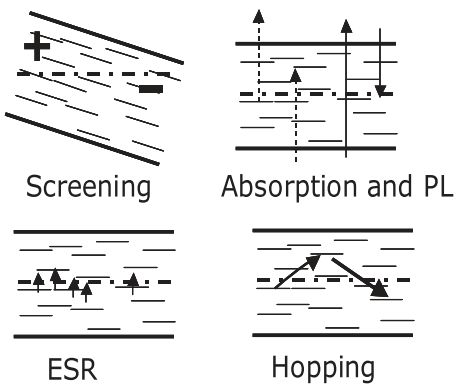

FIG. 2. Sketches of physical processes associated with the one-electron localized states model. Top left: screening in the presence of an applied field due to redistribution of localized electrons to form a dipole. Bottom left: unpaired electrons near the Fermi level (dashed-dotted line) produce a strong ESR signal. Top right: optical absorption of photon energies less then (dashed arrows) and greater than (solid upward arrow) the gap, and photoluminescence (downward arrow) possible at mid-gap energies—solid arrows show what is observed in chalcogenide glasses. Bottom right: hopping conduction via states near the Fermi level. The one-electron localized states model cannot consistently account for the data on chalcogenide glasses.

The conflicts arise when the above model is applied to chalcogenide glasses. It was observed that similar to a-Si, strong screening of the electrostatic field takes place, thus testifying in favor of a high DOS in the mobility gap (top left diagram in Fig. 2). On the other hand, the ESR signal is practically absent, thereby challenging the illustration in the left bottom diagram and shedding doubt on the presence of localized states in the mobility gap. However, a strong ESR signal can be induced by well-absorbed light; this photo-ESR is consistent with the hypothesis of a high DOS in the mobility gap. The optical transitions shown with dashed arrows in the top right diagram were not observed, suggesting that there may be no states in the gap. Instead, the transitions shown with solid arrows were observed, one of which corresponds to the interband absorption (not requiring localized states), while another one, downward, represents photoluminescence (PL) with energies around $\hbar\omega = G/2$. The latter implies a high concentration of localized states close to the Fermi level. Finally, as opposed to the case of a-Si, no hopping conduction was observed in chalcogenide glasses,[12] testifying against the model of a high DOS in the gap.

As a result, the group of observations against a high concentration of localized states includes: lack of ESR signal, absence of hopping conduction, optical gap G_0 approximately equal to the mobility gap G, and relatively low absorption of photons with energy less than G. On the other hand, the group in favor of a high concentration of localized states includes: strong photoinduced ESR corresponding to the electron concentration $\lesssim 10^{20}$ cm^{-3}, photoluminescence with energy close to $G/2$, dc screening length revealing a DOS at the Fermi level of $10^{18} - 10^{19}$ cm^{-3}eV^{-1}, strong pinning of the Fermi level close to the mid gap, photoinduced mid-gap absorption, and photoinduced change in the mid-gap photoluminescence. The spectroscopic aspects of these facts are illustrated in Fig. 3.

B. The negative-U model and soft atomic potentials

A solution to the above controversy was proposed by Anderson[39] who put forward the concept of negative-U (negative Hubbard or negative correlation) energy which implies that two identical charge carriers localized at the same center

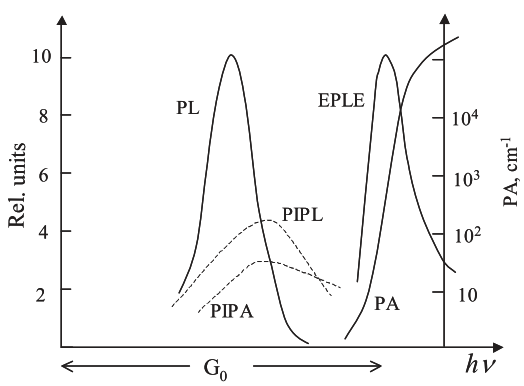

FIG. 3. Sketch of the typical spectroscopic data in chalcogenide glasses: PA, PL, efficiency of photoluminescence excitation (EPLE), PIPL enhancement, and PIPA vs. photon energy $h\nu$. G_0 is the optical gap. All the curves except PA are plotted against the left vertical axis.

will attract, in spite of the Coulomb repulsion. As a result, double occupancy of a localized state becomes energetically more favorable than single occupancy of two localized states, such that the equilibrium occupation is $n = 2$ (electrons or holes), while $n = 1$ can only exist as an excited state. The conceptual leap of the negative-U model in chalcogenide glasses is that electronic-lattice interaction can be so strong that the energy is minimized when a localized state is *double occupied* and surrounded by a self-consistent cloud of lattice deformation.

Since the negative-U model favors two-electron states, it obviously explains the inadequacy of the one-electron model to account for the conflicting observations. For example, the lack of ESR in spite of a high concentration of localized states is due to the fact that the states near the Fermi level are doubly occupied. The photoinduced effects become attributable to the non-equilibrium, single-occupancy states excited by higher energy photons. The rest of the above listed observations can be understood when the nature of the negative-U energy is specified as being related to an abnormally strong electron-lattice interaction for localized charged carriers.

The energy of $n = 0, 1, 2$ localized carriers is described as

$$E_n(x) = nE_0 + kx^2/2 - nQx + U_c\delta_{n,2}, \tag{1}$$

where E_0 is the bare energy of the center, x is the lattice deformation around the center, k is the corresponding spring constant, Q is the deformation potential for the localized carriers, and U_c is the Coulomb repulsion energy applicable when $n = 2$. The dependencies in Eq. (1) are illustrated in Fig. 4. It should be understood that the bare energy levels E_0 are always present as unoccupied states near the mobility edge while states E_1 and E_2 are created by the lattice deformation that occurs when a bare energy level becomes occupied. Therefore, states E_1 and E_2 do not exist in and of themselves but, rather, they are modified versions of the E_0 state.

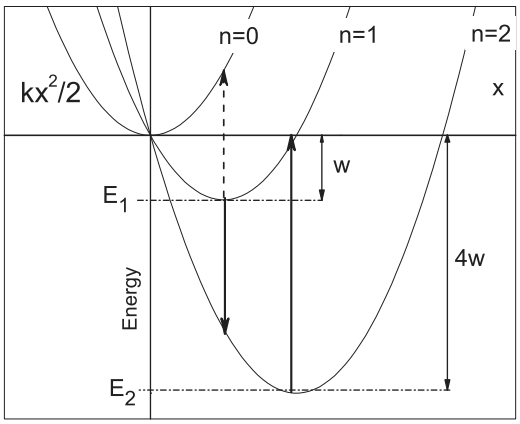

FIG. 4. Energies of n localized charge carriers vs. the local lattice deformation x. The upward solid arrows represent absorption and the downward solid arrows represent photoluminescence processes; the dashed arrow indicates photoinduced photoabsorption from the nonequilibrium $n = 1$ state. E_1 and E_2 represent the equilibrium energies for $n = 1$ and $n = 2$ localized carriers. w is the polaron shift and U_c is assumed to be relatively small.

The equilibrium energies are given by the equation,

$$E_n = nE_0 - n^2w + U_c\delta_{n,2} \quad \text{with} \quad w \equiv \frac{Q^2}{2k}, \tag{2}$$

where w is called the polaron shift which quantifies the strength of electron-lattice interactions. From Eq. (2), the correlation energy is given by

$$U \equiv E_2 - 2E_1 = -2w + U_c. \tag{3}$$

The postulated negative value of the correlation energy corresponds to a strong polaron effect with $w > U_c/2$.

By the Franck-Condon principle, the characteristic energy of the absorbed light in Fig. 4 is $|E_2|$ while that of emission (PL) and photo-induced absorption is $2|E_1|$, and, assuming U_c relatively small, $|E_2| \approx 4|E_1|$, consistent with the data in Fig. 3. These transitions are shown in Fig. 5 with respect to the mobility gap. Note a significant Stokes shift (difference between the absorbed and emitted energies) approximately equal $G/2$ caused by the strong electron-lattice interaction. Comparing Figs. 3, 4, and 5, enables one to estimate $w \approx G/4$ (although w can be somewhat different for the cases of electrons and holes[12]). Also, note that thermal and optical transitions correspond to different positions of the energy levels in the mobility gap (see Fig. 5). The reason for this difference is that optical transitions occur at rates that are too rapid for lattice deformations to occur while thermal transitions allow sufficient time for the lattice to relax, resulting in a change of the energy level before the transition occurs. These differences illustrate the importance of electron-lattice interactions and how the deformations affect the properties of glasses.

Drawing similar energy levels for holes and allowing for some dispersion leads to the right diagram in Fig. 5 that explains how the Fermi level is pinned by a high concentration of 2e and 2h states, forming a gapless spectrum of two-particle excitations. In addition to the pinning (2e, 2h) states, shown in the same diagram are band tails possessing the characteristic decay scales on the order of several hundredths

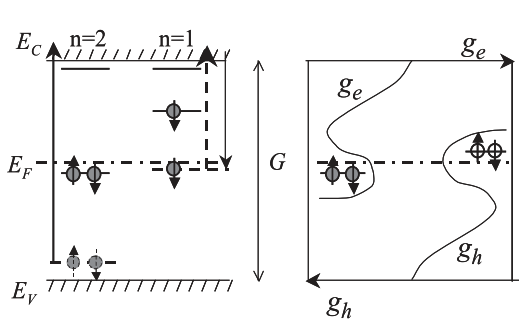

FIG. 5. Left: one-particle energy levels (i.e., energy per particle) corresponding to $n = 2$ and $n = 1$ electrons in the mobility gap. The levels without electrons represent the bare energy. Solid and dashed lines indicate thermodynamic and optical energy levels, respectively. The dashed electron level close to the valence band edge represents the energy needed to optically ionize the 2e state (solid upward arrow); the solid level close to the midgap represents the energy needed to thermally ionize the same 2e state. The arrows have the same meaning as in Fig. 4. Right: density of the 2-electron (g_e) and 2-hole (g_h) states vs. their one-particle energies where negative-U centres near the Fermi level provide its pinning.

of eV. They can contribute to optical absorption and act as shallow traps underlying dispersive transport and other phenomena.[40] As shown in Fig. 5, the one-particle excited states 1e and 1h are obtained through the partial ionization of (2e, 2h). Possessing energies of approximately $w = G/4$ from the corresponding mobility edges, they can affect transport phenomena.[41]

C. The nature of negative-U phenomenon

The microscopic nature of negative-U centers is not particularly important for the purposes of this work; here we limit ourselves to a brief comment on the subject. We note that the negative-U phenomenon can be simply illustrated in terms of a mechanical analogy with two electrically charged balls, each of weight Q, that can be attached to either two different elastic springs or one such spring, as depicted in Fig. 6. The spring elongations represent lattice deformations and the potential energy of the springs is related to the polaron shift w. The scenario with two charged balls on one spring turns out to be energetically favorable when $w > U_c/2$. A related generic interpretation of pairing in terms of the number of electrons occupying a dangling bond, as shown in the bottom row of Fig. 6, does not explicitly show the lattice deformation.

Street and Mott[42] proposed a microscopic model where 2e and 2h states correspond to certain defect states (D^- and D^+), while 1e and 1h is the same dangling bond (D^0). Kastner *et al.* and Kastner and Fritzsche[43] introduced more specific consideration taking into account the chemical nature of chalcogenide forming atoms; in their popular notation D^- and D^+ are represented as C^{1-} and C^{3+} where the superscript indices refer to defect coordination numbers. We note that conceptually similar models of structural defects in chalcogenide glasses continue to be proposed up to this day,[44] without much attention to the anomalous polaron shift underlying the observed gigantic difference between the energies of absorption and emission.

Later work[40,45–47] emphasized that a theoretical description of the negative-U must explain the observed strong Stokes shift and, hence, the underlying significant polaron shift w. The required shift was attributed to centers with abnormally small spring constants k (soft atomic potentials) that exist in glasses due to their inherent structural disorder. Qualitatively speaking, the soft atomic potentials represent small pockets of a very soft liquid-like phase arrested during the vitrification process in the macroscopically solidified glassy structure. Because they are abnormally soft, these small inclusions interact abnormally strong with the charge carriers giving rise to the abnormally large polaron shifts.

The random nature of a glass structure implies that the local spring constants are continuously distributed as illustrated in Fig. 7. Correspondingly, there exists a continuous distribution of local polaron shifts w including those responsible for the states in the proximity of the Fermi level. In particular, the polaron shift $w \approx G/4$ implies the spring constant $k_G \approx \langle k \rangle (2\langle w \rangle / G) \ll \langle k \rangle$ where $\langle w \rangle \lesssim 0.1$ eV is the average polaron shift corresponding to the average spring constant $\langle k \rangle$ which describes the macroscopic properties of glasses. We note that the same concept of soft atomic potentials has successfully explained the presence of atomic double well potentials (DWP) and localized quasiharmonic local vibrations in glasses.[46–48]

A comment is in order regarding the region of very small spring constants, k, which may seem to result in the infinitely large polaron shifts capable of localizing many ($n > 2$) charge carriers in the same microscopic region. It should be understood in this connection that for small enough k, the harmonic approximation for atomic potential fails and anharmonic terms become important. In fact, the soft atomic potentials are described by the expression,[40,45–47]

$$V(x) = \frac{kx^2}{2} + Bx^3 + Cx^4, \tag{4}$$

where k and B are random quantities much smaller than their average values, while C is about its average (finding all the parameters noticeably off their respective average values would be extremely unlikely). It follows that the harmonic approximation is limited to $k > k_h \equiv (2Q^2C)^{1/3}$. For lower k, the anharmonic term Cx^4 would govern the electron autolocalization, and for $k \ll k_h$, the term $kx^2/2$ in Eq. (1) should be replaced with Cx^4, which results in the maximum polaron shift $w_{max} \approx 0.5(Q^4/C)^{1/3}$ not strong enough to allow the many carrier localization.

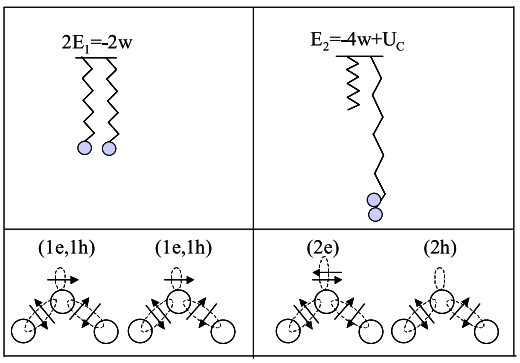

FIG. 6. Mechanical analogy of the negative-U effect consisting of two elastic springs and two charged balls that can be attached to the springs either separately or together (top row) and its simple model based on the valence bonds representation (bottom row) where two electrons can occupy the states of two broken bonds or one dangling bond. The right column is energetically more favorable when $w > U_c/2$.

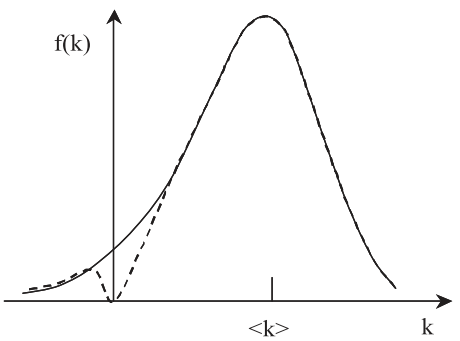

FIG. 7. Probabilistic distribution of the local spring constants in a glass. The gull-wing singularity at the origin (not particularly important in this context) reflects the instability of very soft potentials with respect to small perturbations.[47]

An important conceptual difference between the "defect models"[42,43] and that of soft atomic potentials[40,45–47] is that the latter concentrates on the gigantic polaron shift that underlies the negative-U phenomenon, while the "defect models" explain negative-U by means of specific defect electronic orbitals, leaving the observed gigantic Stokes' shift as an additional (postulated) property beyond that explanation. However, the existence of gigantic polaron shift already explains the negative-U phenomenon [see Eq. (3)], making the "defect models" excessive.

Another important feature of the soft-atomic-potential approach is that it deals with a continuous distribution of spring constants k having a tail down to $k_G \ll \langle k \rangle$, as illustrated in Fig. 7. Correspondingly, it assumes a considerable concentration of localized states between the mobility edges and the Fermi level for which the polaron effect is greater than the average but not as strong as required by the condition $U < 0$. Such states can show up under significant illumination by localizing unpaired electrons and holes, which can explain the observed photo-induced ESR, as well as the features of photoinduced PL (PIPL) and photoinduced photoabsorption (PIPA) in Fig. 3.

D. Electronic transitions with negative-U centers

It should be remembered that the 2e and 2h gapless excitations typically have extremely long relaxation times related to the necessity of carrying a heavy polaron cloud (i.e., atomic deformation) in the course of electron transitions. Here we will describe such slow transitions in terms of electronic DWP with a transition barrier W_B related to the polaron shift. The two minima of such a DWP will correspond to the charge states (0,0) and (2e, 2h) of two centers with energies close to the Fermi level. Another term for DWP is "two-level-system" (TLS).

To estimate the barrier height W_B for the electronic DWP, we consider in more detail the process of transformation from the (0,0) to (2e, 2h) state of the two centers. We start with the (0,0) state, taking 2 electrons from the valence band up to conduction band which requires the energy loss of 2G. Placing them and the remaining two holes at their respective bare levels (very close to the band edges, see Fig. 5) results in a rather insignificant energy gain which we neglect here. Finally, letting the lattice locally deform will deepen the (one-particle) energies at the centers by $\approx G/2$ and, when multiplied by the $N = 4$ carriers involved, this leads to the energy gain of 2G. Overall, the total energy change is zero, while the maximum energy increase in the course of transition was $W_B = 2G$, which we identify with the DWP barrier height.

The rather large barrier of $W_B = 2G$ exponentially reduces the electron transition rate since it is proportional to $\exp(-2G/kT)$. Physically, the latter exponential is attributable to the low probability for thermal fluctuations to create the strong lattice deformations (polaron cloud) that must accompany such electronic transitions (we do not discuss here the low temperature effects that are governed by the zero point vibration energies instead of kT).

Hence, although there exists a high density of localized states near the Fermi level, hopping between those states is extremely doubtful due to the above described deformation related transition barrier $W_B \approx 2G$ (first estimated by Phillips[49]). The barrier is high enough to fully suppress dc hopping conduction that could occur through electron hopping between centers separated by distances on the order of the average inter-center distance.[12] Assuming for specificity $2G \approx 1.6$ eV for the case of GST glasses and implementing the standard estimates[12] yields the multiplier $\exp(-2G/kT) \sim 10^{-27}$. This predicts hopping conduction many orders of magnitude below what is observed in the non-glassy semiconductors (such as a-Si).

From another perspective, we note that if hopping conduction did occur in chalcogenide glasses it would have to proceed through the above described excitations which occur within the mobility gap via the negative-U centers near the Fermi level with their associated lattice deformations. On the other hand, band conduction is an interband mechanism which forgoes the restrictive lattice deformation process. Therefore, the conductivity for band conduction retains the thermally activated factor $\exp(-G/kT)$.

Because the strong polaron effect suppresses dc hopping conduction down to insignificant values, it is worth explaining here the difference between that effect and the known phenomenon of small polaron transport in some materials.[50–52] The latter phenomenon implies materials with translational symmetry, in which no defects are required to create the self-trapped state of an electron in a strongly deformed or polarized lattice; such a state is called polaron. Because of the translational symmetry, polarons must have the ability to move in a system without energy dissipation. This is achieved through the coherent dynamics of the electron and its surrounding deformation. This results in band polaron transport where the polaron bandwidth is exponentially reduced (compared to that of bare electrons) by the probability of coherent lattice translation. In covalent systems with relatively small degree of ionicity, characteristic of chalcogenide glasses, the prevailing mode of electron-lattice interaction is the lattice deformation in the form of local increase or decrease in specific volume. That deformation creates (through the deformation potential) a potential well for the electron decreasing its energy and thus making polarons possible. In the total balance of polaron energy, the electron energy gain is considered proportional to the deformation and the electron density; the elastic lattice contribution is quadratic according to Hooke's law and similar to our earlier expression in Eq. (1).

A significant difference between the settings of Eq. (1) and that of polaron theory is that the latter starts with a fully delocalized electron in an undeformed lattice. Because the corresponding electron density, it is infinitesimally small, it does not interact with the lattice. To achieve a strong enough interaction, the electron wave function must be made strongly localized. That takes a considerable energy of the order of the electron bandwidth. As a result, there is a threshold energy (barrier) to overcome in order to form a small radius polaron; thus, it is more likely to occur in extremely narrow band materials.[50,52]

Chalcogenide glasses do not belong to the class of narrow band materials suitable for small polaron formation.

Instead, the negative-U centers are formed at lattice imperfections: structural defects, weak atomic potentials, fluctuations in lattice parameters, etc., which are supposed to provide the electron localization making up for the above mentioned threshold energy. Because the corresponding strong polaron effect takes place at rare, special, local regions in a glass, no polaron-like band transport is observed here.

In the estimate of the transition barrier between two negative-U centers, we have neglected both the quantum contribution caused by the overlap of the wave functions of spatially close 2e and 2h centers and the Coulomb interaction of 2e and 2h pairs. It was shown[53] that both corrections are significant for the case of *spatially close* pairs, sometimes called intimate pairs, which can decrease the barrier height by several times. In particular, the intimate (2e, 2h) pairs partially decrease their energy due to the strong Coulomb interaction, which relaxes the requirement of very soft atomic potentials with $k \approx k_G$. Because higher k values result in smaller w, the factor $\exp(-2G/kT) \approx \exp(-8w/kT)$ describing the suppressing effect of a polaron cloud on the electronic transition becomes less significant, allowing for much higher hopping probabilities. However, we note that since the magnitudes of the latter and quantum effects depend on the details of the atomic and electronic structure of negative-U centers, our knowledge about W_B for such compact pairs remains rather approximate.

Lacking more accurate information, one can resort to the data[54,55] on alternating current (ac) conduction in chalcogenide glasses that are comparable to that of other noncrystalline semiconductors at relatively low frequencies ($\omega \gtrsim 1$ kHz). Because ac conduction is attributed to electron hopping between close centers,[54] these observations can be explained assuming that the electron transitions in *close pairs* of negative-U centers are as efficient as in the pairs of centers without a strong polaron effect, such as in a-Si. The assumed effectiveness of the electronic transitions in close pairs can be explained[53] by significant suppression of the transition polaron-related barrier in intimate pairs. Qualitatively, such a suppression is due to a substantial spatial overlap of the polaron clouds of two close centers, which makes it unnecessary to fully dissipate and recreate a polaron cloud in the course of electronic transition. The fact that no dc hopping was observed in chalcogenide glasses[12] signifies that no barrier suppression takes place for the centers at distances close to the average.

More specifically, the experimental data on the ac conductivity $\sigma(\omega)$ of chalcogenide glasses exhibit the following behavior.[54,55] The low $T \lesssim 100$ K region is described by $\sigma \propto \omega$ independent of T. In the range of $T \gtrsim 100$ K, the index s in the observed dependence $\sigma \propto \omega^s T^m$ decreases with T. This occurs when the index m is already considerably greater than unity. At yet higher $T \gtrsim 300$ K, there is a peak in the temperature dependence of conductivity. Its position is frequency dependent, $T \propto |\ln(\omega\tau_0)|^{-1}$ where $\tau_0 \sim 1$ ps is the characteristic reciprocal frequency of atomic vibrations.

The above observations are consistent with the picture of close pairs of negative-U centers. The low temperature behavior is typical of TLS. Assuming that tunneling transitions dominate, it was specified[53] for the case of spatially close negative-U centers in the form (in the present notations),

$$\sigma(\omega) \approx \frac{\pi}{3}\omega P d^2, \tag{5}$$

where P is defined in Eq. (10) below for $\tau = 1/\omega$ and d is the dipole moment estimated as $2ea$ with a being the characteristic interatomic distance. The observations show indeed that d is considerably larger than the value expected for atomic TLS.

For higher T, when activated hopping dominates the electronic transitions, the above mentioned indexes s and m were predicted in the form,[53]

$$s = 1 - \frac{6kT}{2G + kT\ln(\omega\tau_0)}, \quad m = 1 - (1-s)\ln(\omega\tau_0), \tag{6}$$

consistent with the observations, where it should be taken into account that $\ln(\omega\tau_0) < 0$.

Finally, the peak in $\sigma(\omega)$ at higher T can be explained by strong correlation in the distribution function of spatially close $2e$, $2h$ pairs formed at the glass transition temperature, T_g, leading to a cut off in that distribution function.[66]

The activation relaxation time for the electronic DWP formed by a pair of negative-U centers can be estimated as

$$\tau = \tau_{min}\exp\left[\frac{2R}{a} + \frac{\Delta W_B(R)}{kT}\right], \tag{7}$$

with

$$\tau_{min} = \tau_0\exp\left[\frac{W_B(R_{min})}{kT}\right] \tag{8}$$

and

$$\Delta W_B = W_B(R) - W_B(R_{min}), \quad (\Delta W_B)_{max} \approx 2G, \tag{9}$$

where R is the intercenter distance, a is the electron localization radius at the center, $\exp(2R/a)$ describes the electron tunneling, and $W_B(R_{min})$ is the activation barrier for intimate pairs separated by the distance $R_{min} \sim a$. Because R is a random quantity with the probabilistic distribution $4\pi R^2 N_U$ where N_U is the concentration of negative-U centers, the probabilistic distribution of relaxation times becomes

$$\rho(E,\tau) = \frac{P}{\tau}, \quad P \approx \frac{\pi N_U^2 a^3}{4\Delta E_U}\frac{[\ln(\tau/\tau_{min})]^2}{1 + 2G/kT}, \tag{10}$$

where we have used a rough estimate $dW_B/dR \sim (\Delta W_B)_{max}/a$ and where ΔE_U is the total energy width of the negative-U center distributions that are approximately uniform in the proximity of the Fermi level. Neglecting the logarithmically weak dependence of P vs. τ, it can be treated as a constant.

For numerical estimates we use the values discussed in Sec. 9.4 of Ref. 12, which suggest $N_U \sim 10^{17} - 10^{18}$ cm^{-3} and $\Delta E_U \sim 0.025$ eV, yielding $P \sim 10^{15} - 10^{17}$ eV^{-1} cm^{-3}. The transition time τ corresponding to the typical $a \sim 10$ Å, average $R \sim N_U^{-1/3}$, and $W_B \approx 2G \sim 2$ eV turns out to be

TABLE I. Listing of each conduction mechanism along with the related analytical expression and estimated field range of applicability. The current I is given in terms of the electric field F, with the pre-exponential $I_0 \propto (-E_a/kT)$. The parameters are defined as follows: k is the Boltzmann constant, T is temperature, q is the elementary charge, ε is the dielectric constant, a is the inter-center distance, $\hbar$ is the reduced Planck's constant, m is the effective carrier mass, $kT_{ph} \sim 0.01 - 0.03$ eV is the characteristic phonon energy, E_0 is the characteristic decay of the density of tail states $g = g_0\exp(-E/E_0)$, where E is energy, L is thickness, $\lambda \approx -\ln(g_0 kTaL^2) \gg 1$ (here, g_0 is the density of localized states), α is the electron localization radius, E_F is the Fermi energy, $\eta \sim 1$ is a numerical factor, $L_c \sim 10$ nm is the percolation cluster correlation radius, r_c is the order parameter, r_x is the crystallite radius, V_{max} is the maximum percolation transport barrier, and $\Delta \sim 0.4$ eV is the band offset between crystalline and amorphous phases.

Mechanism	$\ln(I/I_0)$	Field Range (V/cm)
Poole-Frenkel 1-center activation	$\frac{2}{kT}\sqrt{\frac{q^3F}{\varepsilon}}$	$10^4 - 10^5$
Poole-Frenkel 2-center activation	$\frac{aqF}{kT}$	$< 10^4$
Poole-Frenkel 1-center tunneling	$\frac{\hbar q^2F^2}{3m}\left(\frac{1}{kT}+\frac{1}{kT_{ph}}\right)^2$	$> 10^5$
Schottky emission	$\frac{1}{kT}\sqrt{\frac{q^3F}{\varepsilon}}$	n/a
Delocalization of tail states	$\left(\frac{\hbar qF}{\sqrt{m}}\right)^{2/3}\left(\frac{1}{kT}-\frac{1}{E_0}\right)$	$\sim 10^5$
Space-charge limited currents	$\frac{\varepsilon F}{2\pi Lqgk T}$	$\sim 10^4$
Optimum channel hopping, thin films	$-\sqrt{\frac{8L\lambda}{\alpha}}+1.6\sqrt{\frac{qFL}{kT}}$	$< \frac{E_F}{qL}$
Optimum channel field emission	$-\sqrt{\frac{8\lambda E_F}{\alpha qF}}$	$\gg \frac{E_F}{qL}$
Percolation band conduction	$\eta\sqrt{\frac{L_cqF}{kT}}$	$> 10^4$
Percolation band conductionthin films ($L < L_c$)	$\eta\sqrt{\frac{L_cqF}{kT}} + \frac{L_c-L}{2r_c}\left[\ln\left(\frac{V_{max}}{kT}\frac{2r_c}{L}\right)+1\right]$	$> 10^4$
Crystalline inclusions (1)	$\frac{2\varepsilon}{kT}\sqrt{\left(\frac{r_x\Delta}{q}\right)^3F}$	$10^5 - 10^6$
Crystalline inclusions (2)	$\frac{\varepsilon r_x^2F\Delta}{qkT}$	$< 10^5$

long enough ($\sim 10^{17} - 10^{25}$ s) to fully suppress hopping conduction.[49] Indeed, the latter can be estimated as $\sigma \sim e^2/(\tau kTR) \sim 10^{-26} - 10^{-34}$ Ω^{-1} cm^{-1}, much less than the experimentally observed $\sigma \gtrsim 10^{-3}$ Ω^{-1} cm^{-1}. We note that the frequency-dependent ac conduction at $\omega \gtrsim 1$ kHz is yet far enough from the limiting case of low frequencies bordering the dc regime: the latter would take place for $\omega \sim 1/\tau \sim 10^{-17} - 10^{-25}$ Hz. This range of incredibly small frequencies is due to the strong polaron effect that exponentially slows down the electronic transitions.

On the other hand, spatially close (intimate) pairs can have much lower W_B and exponentially shorter relaxation times than the average distant pairs, thus making noticeable contributions to the system noise[56] and ac transport in a broad range of relatively low frequencies. Another important property of intimate pairs is that they can form untypical chains between the electrodes of very thin samples (see Sec. IV F). The distance between the centers in such chains will be much shorter than the average making them rather efficient channels for dc conduction. Therefore, one can expect that extremely small devices can exhibit transport properties significantly different from their larger counterparts. We shall see in what follows that such untypical transport can dominate conduction in the range of thickness well below 10 nm.

IV. SURVEY OF CONDUCTION MECHANISMS

Sections IV A–IV H provide the physical basis, analytical expressions, and limiting assumptions for various non-ohmic conduction mechanisms. A summary of the expressions for the conductivity in each case is provided in Table I.

A. Poole-Frenkel effect

The originally suggested physics of the PF effect is the decrease in the ionization energy of a single coulombic potential well in the direction of an applied field (explaining $\ln I \propto \sqrt{V}$) or that of a pair of coulombic centers (explaining $\ln I \propto V$), as illustrated in Fig. 8. The corresponding barrier change δ increases the center ionization rate, proportional to which are the free carrier concentration and the activated electric current $I/I_0 \propto \exp(\delta/kT)$. The underlying assumption of a coulombic attractive potential is justified by its ability to give the required decrease in the ionization energy $\delta \propto F$ or $\delta \propto \sqrt{F}$.

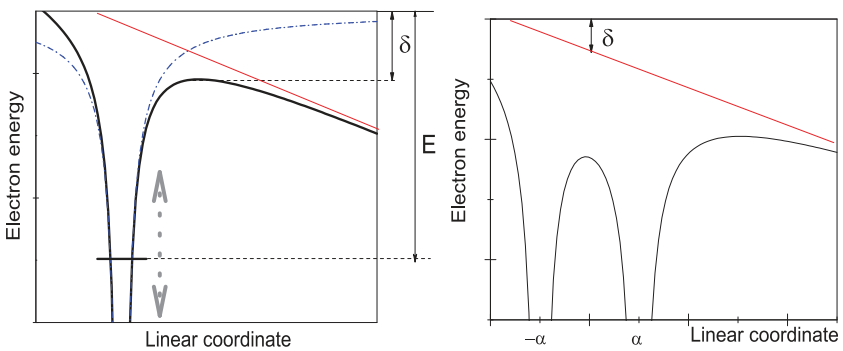

FIG. 8. Left: Field induced decrease δ in activation energy of a coulombic center. Dashed lines show zero field case, tilted red line represents the electric potential of a uniform field. Gray arrow shows vibration of the electron energy E due to electron-phonon coupling. Right: Field induced decrease δ in activation energy of a pair of coulombic centers.

We note that as originally proposed,[14] this mechanism was meant to explain the data on noncrystalline materials (mica, SiO_x, etc.; see Ref. 13 and references therein). Surprisingly, the data on non-ohmic conduction in doped crystalline semiconductors are typically described by other dependencies,[57] despite the fact that the coulomb nature of the defects therein is well established. Therefore, the empirically observed relevance of PF-type dependencies to noncrystalline materials may suggest that their nature is more related to disorder effects rather than individual or pairs of coulomb centers. From that point of view, the PF mechanism may be significantly over-emphasized.

For the case of two centers separated by distance $2a$ in the electric field of strength F, the electron energy along the axis is given by

$$U(x) = -\frac{q^2}{\varepsilon(a-x)} - \frac{q^2}{\varepsilon(a+x)} - Fqx, \tag{11}$$

where q is the electron charge, ε is the dielectric permittivity, and x is measured from the midpoint between the two centers. The position of the lowest barrier maximum, $dU/dx = 0$ is determined from the equation,

$$\tilde{x} = \tilde{F}(\tilde{x}^2 - 1)^2 \quad \text{where} \quad \tilde{x} = \frac{x}{a}, \quad \tilde{F} = \frac{F}{4q/a^2\varepsilon}. \tag{12}$$

The original PF result $x = 1 + \sqrt{q/\varepsilon F}, \quad \delta = \sqrt{4q^3F/\varepsilon}$ follows from Eqs. (11) and (12) when $\tilde{F} \gg 1$ (i.e., $F \gg q/4\varepsilon a^2$); however, it remains approximately valid numerically even at $\tilde{F} = 1$. The characteristic field is $4q/a^2\varepsilon \sim 10^5$ V/cm for the typically assumed[12,24] center concentration of $\sim 10^{18}$ cm^{-3}.

In the opposite limiting case of "weak" fields, $F \ll 4q/\varepsilon a^2$, Eqs. (11) and (12) yield $x = a$ and $\delta = qFa$, corresponding to the so called modified PF effect with

$$\ln(I/I_0) = qVa/L, \tag{13}$$

where L is the glass thickness, emphasized in Ref. 24.

The barrier decrease due to the presence of one or two coulombic centers can be calculated directly from Eq. (12) for an arbitrary field at little computational cost. Of course the δ's corresponding to the PF or modified PF effect can also be appropriately interpolated to give a simple expression for the barrier decrease, valid for both low and high fields. This was done in Ref. 37, where it was then applied to a model with the freed electrons participating in hopping conduction.[24] As discussed in Sec. III and to be elaborated upon in Sec. IV E, it is much more efficient for electrons released from such traps to participate in band (rather than hopping) conduction.

The critical field $4q/\varepsilon a^2$ also implies that the notion of "weak" or "strong" fields can be replaced by condition of low or high defect density (as related to a). Thus, for a given field, the PF effect is dominant for a high defect concentration while the modified PF effect pertains to a low defect concentration. In any event, we observe that significant deviations from the standard PF results can be expected under low fields $F \ll 10^4$ V/cm. This significantly narrows the application of the modified PF mechanism in Refs. 24 and 58, also ruling out its role in the switching field region of $F \gtrsim 10^5$ V/cm.

The two-center model that predicts $\ln(I/I_0) \propto V$ in Eq. (13) remains critically vulnerable to the effects of fluctuations. We note in this connection that the work in Refs. 24, 37, and 58 was limited to a system of equidistant coulombic centers. Random fluctuations in their concentration (present in all systems of centers in solids so far explored) will generate random variations of activation energies translating into exponentially broad distributions of ionization rates; variations in center energies will make this distribution even broader. This results in local carrier concentrations that vary exponentially between different locations. A proper framework for analyzing these types of systems would be percolation theory,[59] which is yet to be applied to PF-type conduction (cf., however, Ref. 60).

In Ref. 61, a Monte Carlo simulation was performed which did allow for the inter-center distance to vary randomly within the material. Rather than using the PF effect, a phenomenological parameter is introduced to give a $\ln(I/I_0) \propto \sqrt{V}$ type dependence. The electrical properties of the system remained particularly sensitive to this parameter, the value of which was assigned rather arbitrarily and without physical interpretation.

Quantum tunneling imposes limitations on the activation PF effect. The corresponding analysis by Hill[13] neglects the role of atomic vibrations on tunneling. A more recent analysis[57] that accounts for electron-phonon interactions results in a picture where the electron energy level moves up and down following oscillations of the atomic system to which it is coupled. As a result, the electron tunneling becomes most likely when the electron energy is significantly above its average position (Fig. 8), and the chief exponential term in the non-ohmic current is given by

$$\ln(I/I_0) = \frac{F^2q^2\hbar}{3(kT^*)^2m} \quad \text{with} \quad \frac{1}{kT^*} = \frac{1}{kT} + \frac{1}{kT_{ph}}, \tag{14}$$

where m is the effective mass of a localized charge carrier, which we take to be close to the true electron mass,[62] and kT_{ph} is on the order of the characteristic phonon energy ($\sim 0.01 - 0.03$ eV).

It was shown[57] that the standard PF results become invalid and the effect is better described by Eq. (14) when

$$F > F_t \equiv \sqrt{\frac{2mE}{\hbar^2}}\frac{kT^*}{q}\left(\frac{kT^*}{E}\right)^{1/3}, \tag{15}$$

where E is the ionization energy ($\approx$0.4 eV in $Ge_2Sb_2Te_5$). Using the above numerical parameters, one can estimate $F_t \sim 10^5$ V/cm. We note that the dependence in Eq. (14), rather than the standard PF law, was experimentally confirmed for many crystalline semiconductors even for fields below 10^5 V/cm (see chap. 10 in Ref. 57).

Overall, we conclude that, for the case of GST glasses, the standard PF expression $\ln(I/I_0) \propto \sqrt{F}$ can apply in the field range of $\gtrsim 10^5$ V/cm. For weak fields, $F \ll 10^5$ V/cm,

the modified PF effect $\ln(I/I_0) \propto F$ can give a more adequate description; however, the effects of fluctuations in the local concentration of centers must be taken into account. For the high field region, $F \gtrsim 10^5$ V/cm, quantum effects lead to $\ln(I/I_0) \propto F^2$, predicting an increase in non-ohmicity in the vicinity of the switching field. The above boundaries can be numerically different for other chalcogenide glasses; however, the hierarchy of regimes remains the same, as illustrated in Fig. 1.

Experimental data[17,23,34] has exhibited a sharp increase in current when the field is very close to its switching value 3×10^5 V/cm, however, it would be premature at this stage to attribute it to Eq. (14). Experimental verification of the temperature dependence in Eq. (14) could clarify this issue. Ref. 63 gives an interesting example of how neglecting all the above reservations and conditions can lead to the far reaching conclusions about the distance between electronic traps based on Eq. (13) from the experimentally estimated derivative $d(\ln I)/dV$.

B. Schottky emission

The Schottky effect[64] originates from the image force induced lowering of the interfacial energy for charge carrier emission when an electric field is applied. This leads to

$$\ln(I/I_0) = \frac{1}{kT}\sqrt{\frac{q^3F}{\varepsilon}} \quad \text{with} \quad I_0 \propto \exp(-\Phi/kT), \tag{16}$$

where Φ is the interfacial barrier height between the semiconductor and the contact metal.

The dependence in Eq. (16) was experimentally verified in the field range $\sim 10^4 - 10^5$ V/cm for various junctions of crystalline semiconductors with metals. However, on empirical grounds, it is hard to believe that it can apply to the case under consideration because of the established $\ln I_0 \propto (-E_a/kT)$, where E_a is half the mobility gap in the chalcogenide material and is independent of contact properties. Some studies reveal that the current is independent of polarity and electrode material, which is additional evidence against the Schottky mechanism.[19]

C. Field-induced delocalization of tail states

Similar to the PF mechanism of decreasing the ionization energies of coulombic centers, the electric field can decrease energies of localized tail states in the mobility gap and even destroy them if they are shallow enough. Transforming localized into delocalized states is tantamount to narrowing the mobility gap; this exponentially increases the free carrier concentration and electric conductivity.

The latter mechanism, suggested in Ref. 26, is specific to noncrystalline materials where the presence of band tails is well established. Tail states are related to intrinsic structural disorder of amorphous materials rather than to any specific defects. The disorder creates microscopic variations in the electric potential generated by different structural units in a material and felt by electrons or holes. Some combinations of these microscopic variations form effective potential wells capable of localizing charge carriers.

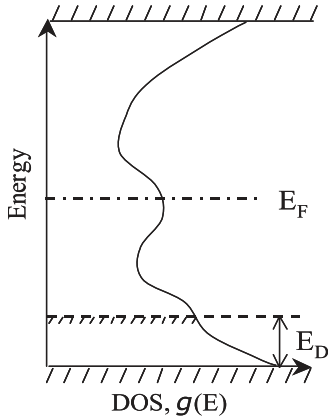

FIG. 9. DOS in the mobility gap of a chalcogenide glass. The electric field shifts the mobility edge for holes up by energy E_D (similar effect for electrons is not shown here).

It was assumed in Ref. 26 that each fluctuation potential well has the same radius r_0 regardless of the energy of its localized state, thus governed only by the well depth. Correspondingly, the condition of the electric field induced delocalization was given in the form $E < E_D \equiv Fqr_0$. Assuming also a simple phenomenological representation of the density of tail states, $g(E) = g_0\exp(-E/E_0)$, the field-induced increase in concentration of charge carriers becomes $n(F) \propto g(E_D)\exp(E_D/kT)$, where the first multiplier describes the decrease in activation energy by E_D, as illustrated in Fig. 9. As a result, the conductivity increases with field as

$$\sigma(F) = \sigma_0\exp\left[Fqr_0\left(\frac{1}{kT} - \frac{1}{E_0}\right)\right], \tag{17}$$

where it is assumed that $E_0 > kT$. The observed temperature dependence in Ref. 26 was consistent with that in Eq. (17).

The above model could be refined by taking into account that the characteristic size of the localized state of energy E is $\hbar/\sqrt{mE}$ and so is that of its corresponding potential well,[65] as illustrated in Fig. 10. As a result, the condition of delocalization, approximately $Fq\hbar/\sqrt{mE} = E$, gives the characteristic delocalization energy $E_D = (\hbar qF/\sqrt{m})^{2/3}$ and, similar to Eq. (17)

$$\sigma(F) = \sigma_0\exp\left[\left(\frac{\hbar qF}{\sqrt{m}}\right)^{2/3}\left(\frac{1}{kT} - \frac{1}{E_0}\right)\right]. \tag{18}$$

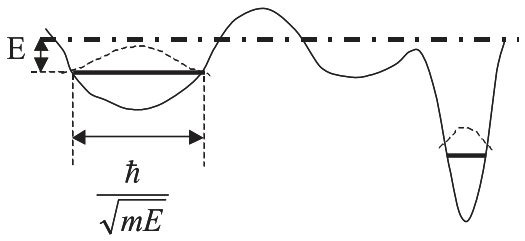

FIG. 10. Localized tail states for the electrons below the mobility edge (shown as dashed-dotted line) have linear dimensions decreasing with energy E in the mobility gap.

This prediction is in a numerically relevant range yielding $E_D \sim 0.1$ eV when $F \sim 10^5$ V/cm.

Further implementations of the theory of disordered systems[65] calls upon using the density of tail states in the form,

$$g(E) = g_0 \exp\left[-\left(\frac{E}{E_0}\right)^{\alpha}\right], \tag{19}$$

where $\alpha = 1/2$ and $\alpha = 2$ for the cases of uncorrelated and strongly correlated disorder corresponding, respectively, to the energies $E \ll \hbar^2/mr_c^2$ and $E \gg \hbar^2/mr_c^2$. If the correlation radius r_c is identified with that of the medium range order in a glass,[66] then $r_c \sim 1$ nm and $\hbar^2/mr_c^2 \sim 0.1$ eV. Using Eq. (19) will obviously modify the results in Eqs. (17) and (18) without changing them qualitatively.

Overall, it may be very difficult—if possible at all (see Sec. V)—to experimentally discriminate between the shapes predicted by Eqs. (17) and (18) or their modifications. What is important is that these predictions pertain to a numerically relevant range $E_D \sim 0.1$ eV when $F \sim 10^5$ V/cm, ensuring strong enough non-ohmicity to explain the observed effects. Also, this model, in contrast to the PF model, gives a natural explanation of why PF-type non-ohmicity [$\ln(I/I_0) \propto \sqrt{F}$ or F] is typically observed in glasses rather than in crystalline materials.

D. Space charge limited current

The exponential current-voltage characteristic can be explained by space charge limited current in a system with almost energy independent density of states.[67] This model is represented in Fig. 11 in the coordinate and energy spaces. Due to low mobility, the charge carriers accumulate in a system (the logarithm of their density is shown in Fig. 11 as the quasi-Fermi level) and create the potential barrier further slowing down their transport. In energy space, charge carriers occupy a layer of certain width δE near the Fermi energy (E_F). Therefore, their charge density is estimated as $\rho = g(E_F)q\delta E$. The corresponding electrostatic potential is $V \approx 2\pi\rho L^2/\varepsilon$ where L is the sample thickness. Expressing from here δE through V and taking into account that the activation energy of conduction is by δE lower than in the ohmic regime, one gets

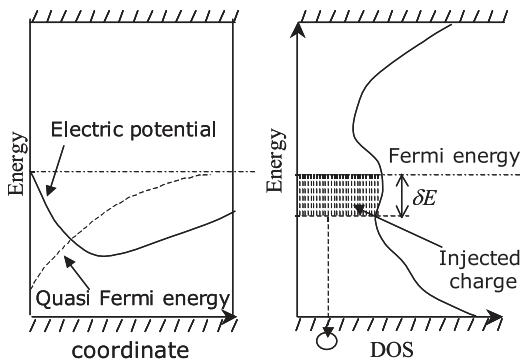

FIG. 11. Left: real space representation of space charge (exponential in quasi-Fermi energy) and electric potential where the barrier top plays the role of a virtual cathode. Right: energy space representation with shaded region filled with injected holes.

$$\sigma = \sigma(0)\exp\left(\frac{F}{F_0}\right) \quad \text{with} \quad F_0 = \frac{2\pi gqLkT}{\varepsilon}. \tag{20}$$

Assuming realistic $g = 10^{17}$ cm^{-3} eV^{-1} and $L = 100$ nm yields a relevant field scale of the non-ohmicity $F_0 \sim 10^4$ V/cm; however that scale strongly depends on the system thickness and density of states, which can make F_0 too large and irrelevant to the observed non-ohmicity in some chalcogenide glasses. The explanation of space charge limited current was put forward in Ref. 28 where F_0 linear in L was observed below room temperature. Near and above room temperature, F_0 was found to be thickness independent.[28,33,34] This data may suggest that space charge limited transport mechanisms play an important role in thicker samples ($L > 1$ μm) below room temperature.

We note that additional verification of the space charge limited mechanism of room temperature conduction in chalcogenide glasses could be obtained from the data on $1/f$ noise measurements. Experimental results[68] show that the corresponding Hooge parameter increases with bias, contrary to what is expected for the space charge limited currents.[69]

E. Hopping conduction

The intent of this section is not to provide a complete description of hopping conduction, since thorough reviews are available elsewhere.[12] Here, we provide a brief explanation as to why hopping conduction was not observed experimentally in chalcogenide glasses.[12,70]

A high density of localized states [g_F] at the Fermi level (E_F) in non-crystalline semiconductors can give rise to hopping transport. The mechanism is based on electronic tunneling ("hops") between localized states that are randomly distributed in real space and energy space.[12,26] In materials where hopping does occur, it dominates at low temperatures (T) and is described by the Mott law[12]

$$\sigma = \sigma_0 \exp[-(T_0/T)^{1/4}], \quad T_0 = \beta/kg_F\alpha^3, \tag{21}$$

where α is the localization radius of the electron wave function, and $\beta \sim 1$ is a numerical factor. However, at room or higher T of practical interest, the primary transport mechanism in bulk materials is typically band conduction.

It has long been established that room temperature conduction in chalcogenide glasses is dominated by band transport.[12] One piece of evidence is that in all chalcogenide glasses the activation energy of conduction is close to half the mobility gap, $E_a \approx G/2$, identified with the Fermi level pinned at that position. As discussed in Sec. III, lack of hopping is explained by the abnormally strong polaron effect for localized charge carriers[12,39,71] requiring electron transitions to be accompanied by the inter-center transfer of atomic deformations (polaron cloud), which exponentially suppresses the probability of hopping. The strong polaron effect makes chalcogenide glasses significantly different from other amorphous semiconductors, such as a-Si, where hopping conduction was experimentally observed.[12,72]

On a more quantitative level, we note that the polaron effect on hopping conduction was explicitly taken into

account in Ref. 74. It was shown [in Eq. (24) of that work] that in the high temperature regime the exponent of conductivity contains both the well known Mott term[12] $(T_0/T)^{1/4}$ and the polaron related term $W/2kT$ with the polaron shift W being close to $G/4$ as explained above in Sec. III. The latter combination cannot be reduced to the observed activation conductivity exponent $\approx G/2$.

Finally, we note a simple estimate showing how hopping cannot provide the high current densities $j \sim 10^4$ A/cm^2 observed in the glassy state of modern PCM,

$$j \sim \frac{q\nu}{R^2}\exp\left(\frac{-E_a}{kT}\right) \sim 5 \quad \text{A/cm}^2, \tag{22}$$

where we have assumed the typical frequency of attempts $\nu \sim 10^{13}$ s^{-1}, inter-center distance $R \sim 10$ nm, and $E_a = 0.4$ eV. For comparison, the devices of area 10^{-10} cm^2 with average current of 1 μA used in Ref. 24, correspond to a current density of 10^4 A/cm^2, decades higher than expected for hopping from Eq. (22).

The latter estimate can be put in a more standard perspective using Mott's criterion of band conduction,[12] according to which the thermally activated conduction $\sigma = \sigma_0\exp(-E_a/kT)$ should have a preexponential in the range $\sigma_0 = 150 - 600\ \Omega^{-1}\text{cm}^{-1}$. The data[75] in Fig. 12 show that the latter criterion is satisfied for the case of GST based PCM. More recent observations[76] confirm the latter conclusion about the band transport conduction in glasses of phase change memory.

Contrary to the above understanding, the authors of Refs. 24 and 58 proposed that conductivity in chalcogenide glasses is due to an altered form of hopping. In that work it was assumed that electrons move without tunneling between equally spaced centers. The same hopping-without-tunneling mechanism was originally proposed for ionic conduction, i.e., for heavy (atomic) classical particles that possess continuous energy spectrum above the barrier.[31,73] For the case of light quantum particles, such as electrons or holes, the spectrum is discrete and may have no quantum states between the barrier and the mobility edge.

The continuous energy spectrum needed for the purely activated transitions assumed in Refs. 24 and 58 starts at the mobility edge. Therefore, the "no-tunneling" activated electronic transitions between the nearest neighbors would have to go via intermediate states at the mobility edge. However, allowing the electron or hole to utilize the states at the mobility edge is inconsistent with hopping conduction. Indeed, carriers at the mobility edge would attain the band mobility, which is well above that of hopping, thus giving rise to band transport and the nearest neighbor concept would not apply. In other words, having activated to the mobility edge, the charge carrier would be capable of traveling considerable distances to other (far from the nearest) traps or even to the device terminals.

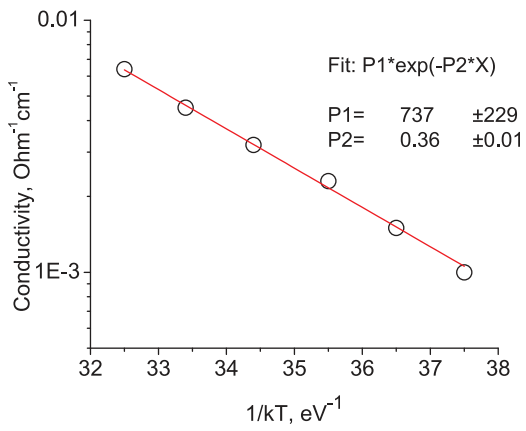

FIG. 12. Temperature dependence of conductivity in a GST based PCM structure.

The above reasoning explains why the hopping-without-tunneling mechanism has never been included in the existing theory of hopping conduction in semiconductors (the possibility of the mobility edge being involved in hopping was a topic of several discussions in the 1970s, as witnessed by the authors of this work, all of which led to negative conclusions).

The work in Refs. 24 and 58 interpreted $E_a \approx G/2$ as the activation energy of hopping to the nearest center, assuming a transition through an intermediate state. In addition, it was assumed that all the inter-center distances are the same, thereby neglecting fluctuations in center concentration and activation energy, which are known to have exponentially strong effects on hopping conduction and determine the temperature and field dependence.[59]

In Ref. 61, hopping between localized states is assumed to occur through direct or thermally assisted tunneling. The transmission coefficient is assumed to have a particular field dependence $\sim\exp(\sqrt{V})$ which varies exponentially on a certain phenomenological parameter. The physical basis for this parameter is not discussed, and it is shown in that same paper that electronic transport is extremely sensitive to its value. The authors, however, point out that different conduction mechanisms (e.g., band transport) need to be included, especially when considering high current densities.

F. Optimum channel hopping

Optimum channel hopping describes the gigantic transverse conduction that has been observed[79] in thin amorphous films. A thorough review of the related work is provided in Ref. 77. Similar to classical hopping conduction discussed in Sec. IV E, optimum channel hopping involves tunneling between localized states but it differs from the classical mechanism in the following ways: (1) optimum channel hopping does not occur on the macroscopically isotropic percolation cluster but, rather, through untypical and nearly rectilinear hopping chains of spatially close localized states; (2) it is characterized by laterally nonuniform (or pinhole) current flow; and (3) it can dominate over typical band transport in systems that are thin enough or subject to sufficiently strong electric fields. For chalcogenides, we consider the possibility that optimum channels can be comprised of localized states that are not subject to strong polaron effects.

Following the approaches in Refs. 77 and 79 we concentrate on optimum channel hopping through short distances via favorable yet sparse clusters of rather rigid localized states that form efficient transport pathways (see Fig. 13).

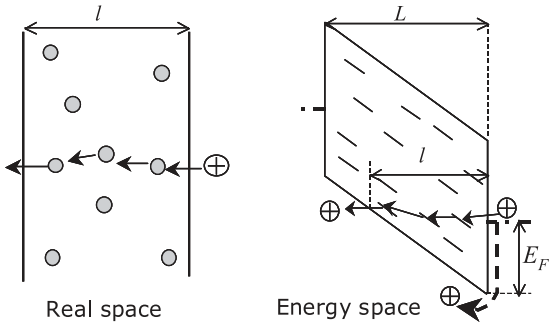

FIG. 13. Left: field emission via hopping through an optimum chain; circles represent localized states. Right: same in the energy space.

The conductivity will be dominated by *optimum pathways* that are a compromise between a high transmission rate and not too low probability of finding the pathways being considered. For the case of thin amorphous films, it was shown[77,78] that optimum channel hopping leads to a transverse conductivity given by

$$\sigma \approx \sigma_0 \exp\left(-\sqrt{\frac{8L\lambda}{\alpha}}\right), \tag{23}$$

where L is the thickness, α is the localization radius, $\lambda \approx -\ln(g_0 kT\alpha L^2) \gg 1$, and g_0 is the density of localized states.

Because Eq. (23) is not widely known to the microelectronics community, we mention here its simplified derivation. Consider a hopping pathway formed by N-center chain of almost equidistant centers. The probability of finding such a chain is estimated as $p^N = \exp(-\lambda N)$, where $\lambda \equiv \ln(1/p)$ and p is the probability of finding one center in the pathway. The probability of hopping through a distance L/N (between two nearest centers in the chain) can be written in the form $\exp(-2L/N\alpha)$, where α is the localization radius on the center. The product of these probabilities $\exp(-N\lambda - 2L/N\alpha)$ gives a partial current through an N-center chain. Optimizing it with respect to N determines the most efficient chains and results in Eq. (23); expressing λ through the density of states takes a more accurate approach.[77]

1. Optimum channels in thin films

For the case of thin amorphous films subject to moderate fields ($F < E_F/qL$, where E_F is the Fermi level), it was shown[77,78] that optimum channel hopping leads to a transverse conductivity given by

$$\sigma \approx \sigma_0 \exp\left(-\sqrt{\frac{8L\lambda}{\alpha}} + 1.6\sqrt{\frac{qFL}{kT}}\right), \tag{24}$$

where the parameters are the same as in Eq. (23). Polaron effects are neglected in Eq. (24) and, therefore, in chalcogenide glasses this form of hopping conduction cannot rely on the typical electronic states near the Fermi level. However, these channels through extremely thin films or in the presence of strong fields (described more in detail in Sec. V) can be formed by untypical spatially close states, for which the effects of polaron cloud are less significant, or they can be formed by states far from the Fermi level having much smaller polaron shifts as explained in Sec. III; for the case of chemically imperfect thin films, hopping in optimum channels could be due to extraneous states formed by certain impurities. Using different terminology, the notion[36] of hopping via optimum channels was alluded to as a mechanism describing the thickness-dependent resistance observed in thin films ($8 < L < 35$ nm). In that work, the strong polaron effects that are characteristic of these glassy systems were not taken into account and no analytical treatment was provided.

2. Optimum channel field emission

The standard interpretation of field emission is based on the model of electron tunneling through a triangular potential barrier with a slope F due to an electric field.[64] Our model here proceeds from the premise of a continuous energy spectrum of localized states in the mobility gap, typical of amorphous materials and capable of giving rise to hopping conduction. Such states lie high enough above the Fermi level that, according to the understanding in Sec. III, they are not related to soft atomic potentials and thus do not posses the strong polaron shift that suppresses hopping. The possibility of hopping transport through such "rigid" states far from the Fermi level is fully compatible with the above-described suppressed hopping at the Fermi level.

For the case[78] of strong fields, $F \gg E_F/qL$, Eq. (23) remains valid with the substitution $L \to l = E_F/qF$ (see Fig. 13 right). As a result, one obtains

$$\sigma \approx \sigma_0 \exp\left(-\sqrt{\frac{8E_F\lambda}{\alpha qF}}\right), \tag{25}$$

which is significantly different from the standard field emission conduction with $\ln(\sigma/\sigma_0) \propto -1/F$.

One qualitatively distinctive feature of the above considered field emission is that it is significantly nonuniform and occurs through rare optimum channels (as opposed to the standard uniform Fowler-Nordheim emission from contacts[64,80]); this may lead to local heating, facilitating structural transformations in chalcogenide glasses. Another feature related to such lateral nonuniformity is that very small area devices, $A \lesssim \alpha L \exp(\sqrt{E_F\lambda/\alpha qF})$, may not have an optimum channel with certainty, in which case their resistances will be determined by the most efficient of available random channels; hence, there will be strong variations between the conductances of nominally identical cells.

Overall, it should be noted that the field emission mechanism can be expected to show up in very thin structures where the hopping resistance corresponding to Eq. (25) is not blocked by a significantly larger resistance of the film in series.

G. Percolation conduction

In general, conductivity of randomly nonuniform materials is described in terms of percolation.[59] This concept

includes both the hopping conduction and band conduction in a medium where charge carrier concentration exponentially varies between different locations due to spatial variations in the electron potential energy. The concept of spatially varying mobility edge can be derived based on the above mentioned picture (Sec. IV C) where a glass band structure is represented by a set of random potential wells with localization/delocalization effects leading to the mobility edges. Some regions will contain predominantly deeper than the average or shallower than the average potential wells corresponding to local variations in the envelope electronic potential in the form of smooth wells or barriers. The latter variations translate into the electric conductivity exponentially varying in space. Experimental evidence of such variations in chalcogenide materials was presented in Ref. 81.

Percolation conduction evolves on a mesh built of material regions with conductivity below a certain critical value $\sigma_c \equiv \sigma_0 \exp(-\xi_c)$ such that the mesh enables a connection between two flat electrodes, regardless of distance L between them. Such a mesh is called an infinite percolation cluster and is characterized by the correlation (mesh) radius $L_c < L$, as shown in Fig. 14.

The topology of the percolation cluster can be pictured as arising from a multitude of sites where the nearest neighbors can be connected with random resistors $R = R_0 \exp(\xi)$. Here ξ is a random parameter. For example, $\xi = E_F/kT$ for the case of band percolation conduction, where E_F represent a random energy distance between the band edge (which is spatially modulated) and the Fermi level. As another example, $\xi = 2\Delta r/\alpha + \Delta E/kT$ for hopping conduction, where Δr and ΔE are the distances between the two centers in the real and energy space, respectively (α being the localization radius on the center). The cluster forming connection proceeds in sequence starting from the minimum resistor ($\xi = 0$) and adding larger ones up to $\xi = \xi_c$, until the everywhere connected cluster is formed. The mesh structure illustrated in Fig. 14 is built of filaments obtained by the series connection of random resistors where the maximum resistor is close to $R = R_0 \exp(\xi_c)$ for each of the filaments.

Following a theory of high-field percolation conduction,[82] each cell of the percolation cluster accommodates voltage $V_c = VL_c/L$. Because the resistors that constitute the filament are exponentially different, the latter voltage almost entirely concentrates on the strongest, first maximum resistor (1-max in Fig. 14). That voltage, concentrated locally, affects the resistance of the element across which it drops. The mechanism of the latter action can depend on the specific system under consideration: changes in center occupation numbers for the case of hopping, or field-induced ionization for the case of band transport. The field affected maximum resistor in the filament decreases its resistance down to the second maximum (2-max in Fig. 14), after which the voltage distributes evenly between the two resistors (1-max and 2-max), modifying both of them, and then extending to the third maximum resistor, etc. Such equalization will sequentially take place in a number of resistors having ξ_i from the maximum one (ξ_c) down to $\xi_0(V)$ defined by the condition,

$$\sum_{\xi_0}^{\xi_c} \xi_i = \frac{qV_c}{kT}.$$

Approximating the sum by the integral gives $(\xi_c - \xi_0)^2 / 2\xi_{max} = qV_c/kT$, where it is assumed that the random parameter ξ is uniformly distributed in the interval from 0 to $\xi_{max} \sim \xi_c$. As a result, the effective conduction is described by

$$\sigma \propto \exp(-\xi_0) = \exp\left(-\xi_c + \sqrt{\frac{2\xi_{max} qV_c}{kT}}\right).$$

Substituting here the definition $V_c = VL_c/L$ and $F = V/L$, one finally obtains

$$\sigma(F) = \sigma(0) \exp\left(\eta \sqrt{\frac{qFL_c}{kT}}\right), \tag{26}$$

where $\eta \sim 1$ is a numerical coefficient.

We observe that the conductivity depends on electric field in a manner very similar to the original PF result. Furthermore, assuming that each resistor has a linear dimension of the medium range order parameter r_c, L_c can be numerically estimated as $r_c(\delta E_a/kT) \sim 10 r_c \sim 10$ nm, where δE_a is interpreted as the amplitude of variations of the activation energy of conduction. It is estimated as the valence band offset between the most conductive (close to crystalline GST) and least conductive amorphous GST regions: $\delta E_a \approx 0.4$ eV. With the above estimate in mind, Eq. (26) predicts significant non-ohmicity starting from $F \sim 3 \times 10^4$ V/cm, in reasonable agreement with observations.

Finally, we note that in the case of very thin films, $L < L_c$, the transversal conduction will be determined by rare, most conductive channels formed by random regions of relatively high carrier concentration, rather than the percolation cluster of mesh size L_c. Assuming that the resistors with $R = R_0 \exp(\xi)$ and $\xi < \xi_L$ are involved, the probability of finding the number $L/2r_c$ of such resistors forming a chain through the film between the electrodes can be written as $\exp[(L/2r_c)\ln(\xi_L/\xi_{max})]$. Dividing the latter by that chain resistance $R_0 \exp(\xi_L)$ gives the partial conductance of chains with $\xi \le \xi_L$. Optimizing the exponent of the latter ratio with

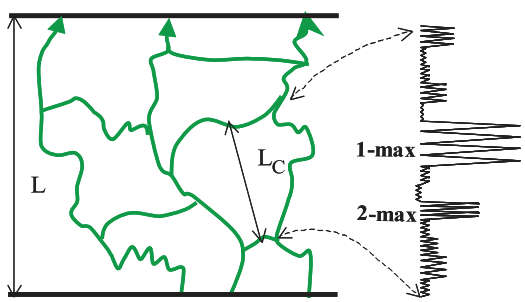

FIG. 14. Left: Fragment of percolation cluster with mesh size L_c in a material of thickness L. Right: equivalent circuit of a filament of the percolation cluster where exponentially different resistors in series are depicted by resistors of different sizes; the first and second maximum resistors are marked for illustration.

respect to ξ_L gives the optimum chain parameter $\xi_L = L/2r_c$. As a result, the conductance of the film can be estimated as

$$\sigma \propto \exp\left\{ -\frac{L}{2r_c}\left[\ln\left(\frac{V_{max}}{kT}\frac{2r_c}{L}\right)+1\right]\right\}.$$

In the latter equation, one can impose the condition $\sigma = \sigma_\infty \equiv \sigma_0 \exp(-E_a/kT)$ when $L = L_c$, where σ_∞ has the meaning of the bulk conductivity. As a result, the effective conductivity of thin ($L < L_c$) structures can be written in the form,

$$\sigma = \sigma(F)\exp\left\{ \frac{L_c - L}{2r_c}\left[\ln\left(\frac{V_{max}}{kT}\frac{2r_c}{L}\right)+1\right]\right\}, \qquad (27)$$

where $\sigma(F)$ is given by Eq. (26). Here we have neglected the difference between logarithmic terms evaluated at L_c and L and have taken into account that $\xi_{max} = V_{max}/kT$, where V_{max} is the maximum transport barrier.

One prediction of Eq. (27) is that the effective activation energy of conduction $E_a = |d\ln(\sigma)/d(1/kT)|$ will decrease as the film thickness decreases below $L = L_c$. Another prediction refers to the case of extremely small devices with area below $A_c \sim r_c^2 \exp\{-(L/2r_c)\ln[(2r_c/L)(V_{max}/kT)]\}$ so that the above defined optimum channel is unlikely to be found within the device area. For such devices, conductance will be determined by the most efficient of the available channels, which will differ between samples; hence, there will be strong fluctuations in conductance between nominally identical devices. According to our rough estimates, that might occur well below the 10 nm scale.

H. Conduction through crystalline inclusions in amorphous matrix

It is known that the reset pulse in chalcogenide PCM melts the material which then cools down fast enough to freeze in the amorphous phase, forming a dome (sometimes called a "mushroom") as sketched in Fig. 15. This melting-to-freezing transition is believed[23,83] to result in a number of crystalline particles embedded in the amorphous matrix. The latter scenario results in an interesting possibility that the system conductance will be governed by potential fluctuations created by the embedded crystallites. We note parenthetically that the presence of embedded crystallites follows from the standard thermodynamic consideration for the case of any glass possessing a crystalline counterpart of lower chemical potential.

Our model is based on the known valence band offset $\Delta \approx 0.4$ eV between the amorphous and crystalline phases (see Fig. 16). According to the standard principles of heterojunction physics, this offset is accommodated by the system through electrostatic screening. The screened potential is described by the standard Poisson equation $\nabla^2\phi = -4\pi\rho$ where the charge density is in turn related to the potential ϕ. That relation depends on the density of electron states $g(E)$, which, following the approach in Ref. 12, we assume constant. This gives $\rho = \phi q^2 g$ and the Poisson equation reduces to

$$\nabla^2\phi = -\phi/r_s^2 \quad \text{with} \quad r_s = 1/\sqrt{4\pi q^2 g}, \qquad (28)$$

where r_s has the physical meaning of the screening radius.

The solution of Eq. (28) for a spherically symmetric case is well known, $\phi \propto r^{-1}\exp(-r/r_s)$. The coefficient in front of it is determined by the boundary condition $q\phi(r_x) = \Delta$, where r_x is the crystallite radius. As a result each crystallite creates a potential,

$$\phi(r) = \Delta\frac{r_x}{qr}\exp\left(\frac{r_x - r}{r_s}\right) \quad \text{when} \quad r > r_x, \qquad (29)$$

$r_s \gtrsim 100$ nm in the typical chalcogenide glasses. We note that the above assumption of constant density of states is not very restrictive as long as we are interested in distances shorter than r_s that is $\phi(r) \approx \Delta r_x/qr$; this can be readily verified for another standard case of a single-level density of states often used for crystalline semiconductors.

The potential in Eq. (29) is the same as that of a coulombic center with effective charge,

$$Zq = \frac{r_x \varepsilon \Delta}{q} \sim 10q.$$

Therefore, one can use the entire wealth of results known for systems of charged centers in semiconductors to derive the following implications:

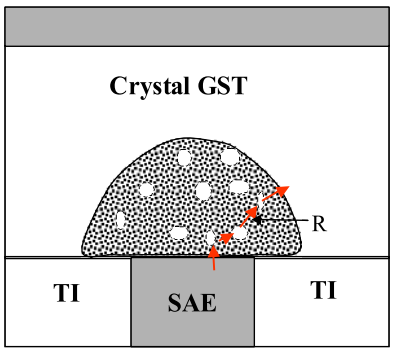

FIG. 15. Amorphous dome with crystalline inclusions as part of the typical PCM structure including a small area electrode (SAE) and thermal insulator (TI). *R* is the average distance between crystallites. Arrows represent the current flow utilizing a path of minimum resistance.

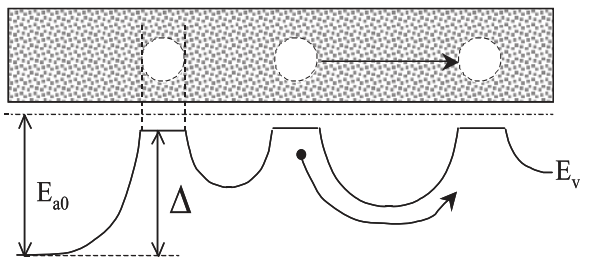

FIG. 16. Top: a fragment of amorphous matrix with embedded crystallites. Bottom: energy band diagram showing valence band edge E_v in the crystalline and amorphous matrix (with offset Δ) and the activation energy E_{a0} is an amorphous phase without crystallites. Dotted-dashed line represents the chemical potential. Arrows show the current flow between two crystallites.

(1) Fluctuations of the electrostatic potential energy exist with the characteristic screening radius r_s and amplitude[59] $\delta U = Zq^2\sqrt{n_c r_s^3}/(\varepsilon r_s)$, where the square root represents the fluctuation in the number of charged crystallites of concentration n_c in a volume of radius r_s. Taking into account the above definition for Z, one can write

$$\delta U \approx \Delta\sqrt{v\frac{r_s}{r_x}}, \tag{30}$$

where $v \equiv n_c r_x^3$ is the volume fraction occupied by crystalline particles. Using the above mentioned parameters it can be rather significant, $\delta U \gg kT$.

(2) The average decrease in the mobility edge, $\delta E_m \approx Zq^2(n_c)^{1/3}/\varepsilon$, can be represented as

$$\delta E_m \approx \Delta v^{1/3}, \tag{31}$$

can be significant as well. The total decrease in activation energy of conductivity due to percolation can be estimated as

$$\delta E_a = \delta E_m + \nu\delta U, \tag{32}$$

where ν is a numerical multiplier of order unity. It is dominated by its fluctuation component δU as long as the average distance between crystallites is shorter than the screening radius, $R < r_s$.

(3) The Poole-Frenkel effect appears here without any additional assumptions about the presence of coulombic centers in a material. The consideration in Sec. IV A will apply with corresponding renormalizations of the center's charge, $q \to Zq$. For example, the critical field of interplay between the regimes of one- and two-center field ionization regimes will become $Ze/4\varepsilon a^2$; numerically, it is $\sim 10^5$ V/cm when the distance between crystallites is $a \approx 10$ nm. The two-center ionization effect results in the current,

$$I = I_0\exp\left(\frac{\varepsilon r_x aF\Delta}{qkT}\right), \tag{33}$$

and the one-center effect becomes

$$I = I_0\exp\left\{\frac{2\varepsilon}{kT}\sqrt{\left(\frac{r_x\Delta}{q}\right)^3 F}\right\}. \tag{34}$$

(4) All the implications of the percolation conduction mechanism in Sec. IV G will be applicable here. One specification is that the correlation length L_c [see Eq. (26)] for a system of charged particles becomes equal to the screening radius r_s. We note that for very small devices with size $L < r_s$, the size will play the role of screening radius.[84] In the latter case, Eq. (26) reduces to $\sigma(V) = \sigma(0)\exp(\eta\sqrt{qV/kT})$.

Overall, the mechanism described in this subsection suggests the important role of the reset characteristics that determine the shape and composition of the amorphous dome in PCM devices. We shall briefly touch upon this issue further in Sec. V below.

V. DISCUSSION

The non-ohmic conduction mechanisms described in this work are listed in Table I along with their characteristic relations and corresponding domains of applicability. Based on the experimental data, the only ones that can be

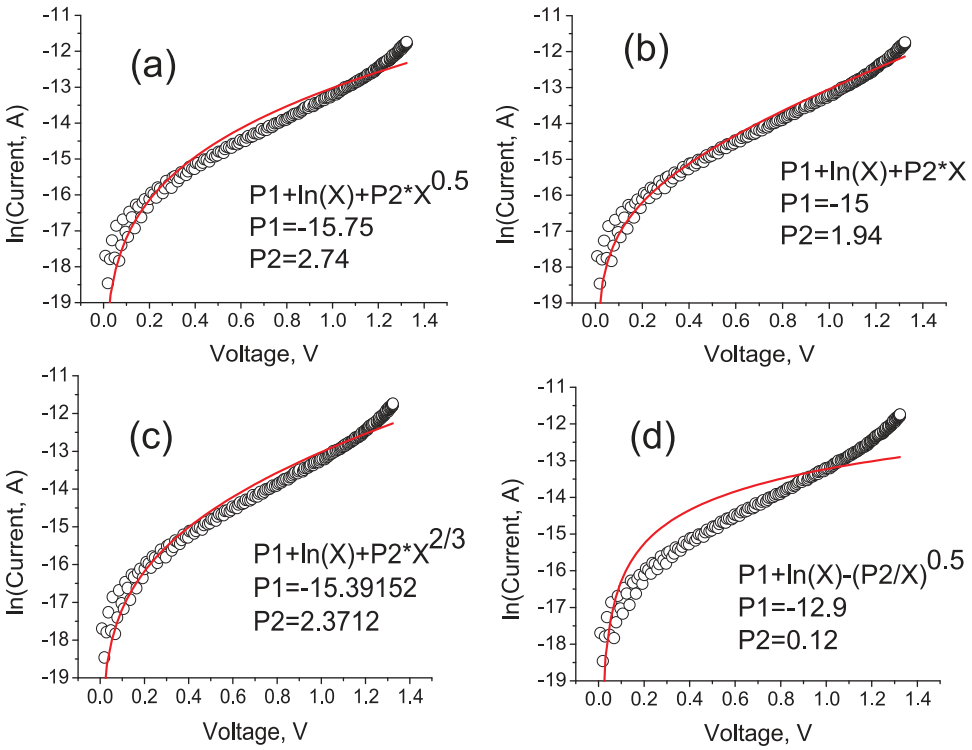

FIG. 17. Four different fits of the same typical IV curve (presented also in Fig. 1) in the reset state of GST based PCM structure corresponding to the expressions discussed in the text: (a) $\ln(I/I_0) \propto \sqrt{V}$, (b) $\ln(I/I_0) \propto V$, (c) $\ln(I/I_0) \propto V^{2/3}$, and (d) $\ln(I/I_0) \propto -1/\sqrt{V}$.

excluded outright are Schottky emission and classical hopping conduction.

Shown in Fig. 17 are examples of typical data fitting corresponding to the various current voltage dependencies of the above discussed models; in each case one fitting equation was used to fit the entire IV curve. It appears that $\ln(I/I_0) \propto V$ provides the best fit, while the fit with $\ln(I/I_0) \propto -1/\sqrt{V}$ is the least successful. We note, however, that the approach implemented in Fig. 17 postulates a single dependence throughout the entire region of voltages. In reality, as we have seen, a single dependence fit may not be adequate: more than one non-ohmic domain with different temperature and thickness dependencies is typically observed, with a faster growing current in the pre-switching region. Eliminating the latter and limiting the single-curve fitting to relatively low voltages, the models (a)-(c) of Fig. 17 fit equally well, while the model (d) remains the least fitting, as illustrated in Fig. 18.

These observations indicate that IV data fitting alone may not be conclusive enough to identify the most adequate model of transport in chalcogenide glasses. As can be seen in Table I, several mechanisms provide the appropriate field dependence within an applicable domain. We note that several transport mechanisms may be appropriate with one mechanism prevailing in a particular domain of electric field, temperature, or thickness. For example, data for thickness dependence suggests that space charge limited current may dominate below room temperature for samples of thickness $L > 1$ μm.[28,33]

A particular example of how fitting alone is inadequate to discriminate between different conduction mechanisms is given by Refs. 24 and 37. In the former work, the modified Poole-Frenkel effect is applied to a model of hopping conduction. Later the authors incorporate the classical PF effect into the same model to better describe the high field region.[37] In looking at Fig. 7 of Ref. 24 and Fig. 3 of Ref. 37 (of seemingly the same IV data), to the eye the fits are identical. This can be explained by the tuning of other parameters (in this case, attempt-to-escape frequency or center concentration). The same articles also provide nearly identical fits of activation energies, indicating that even looking at multiple types of data may be insufficient to discriminate between similar conduction mechanisms.

In our opinion, additional detailed studies are required to discriminate between the different mechanisms listed in Table I. Such facts would include information about the temperature and size dependencies of conduction, resistance noise dependencies, statistical variations between different samples, differences between glasses with and without memory, and possibly some others.

An example of one such indicative fact is the observed dependencies[85] of the threshold voltage V_{th} and threshold current I_{th} on the *ohmic* resistance of the PCM reset state R_{res}, where V_{th} is logarithmic in and I_{th} is the reciprocal of R_{res}. In some devices, those relations may be masked by geometrical or specific design related features. Yet, these results may point at the percolation nature of conduction discussed in Sec. IV G above and are applicable to spatially nonuniform systems, including the case of crystalline inclusions discussed in Sec. IV H. Indeed, according to percolation theory the ohmic resistance is $R = R_0\exp(E_a/kT)$, where E_a is the percolation transport barrier height. Assuming that barrier shape to be parabolic, its linear dimension can be estimated as $l = r_c\sqrt{E_a/kT} = r_c\sqrt{\ln(R/R_0)}$, where r_c is the correlation radius (possibly equal to that of the medium range order). Because most of the voltage drops across that barrier, one can write $V_{th} = lF_{th} \propto \sqrt{\ln(R/R_0)}$, in qualitative agreement with the observations. On the other hand, the usual relation $I_{th} \propto \exp(-E_a/kT) \propto 1/R$ holds.

We now briefly discuss the case of extremely thin devices where optimum channel field emission described by Eq. (25) or percolation conduction in very thin films described by Eq. (27) can apply. Here, we use a possible example of such data from Ref. 36 aimed at studying thickness dependence in the limit of small amorphous volumes in GST PCM cells. From that data, we have plotted the resistance R as $\ln(R/R_0)$ vs. $\sqrt{L}$ for thicknesses between 8 and 35 nm. As show in Fig. 19, Eq. (25) provides good agreement with the data which is indicative of the optimum channel field emission mechanisms (see Sec. IV F 2). However, as mentioned in Sec. II, the thickness values were not directly measured but were inferred from IV measurements using a modified PF model. On the other hand, the amorphous thickness was varied by varying the reset pulse, which can also affect the crystal fraction in the resulting amorphous region. In that

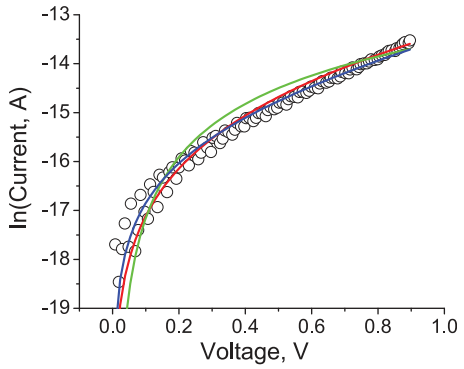

FIG. 18. Fitting the data of Fig. 17 in the domain of $V < 1.0$ V, which excludes the steep increase near threshold. The models with $\ln(I/I_0) \propto \sqrt{V}$ and $\ln(I/I_0) \propto V$, fit equally well, while that of $\ln(I/I_0) \propto -1/\sqrt{V}$ remains outstanding.

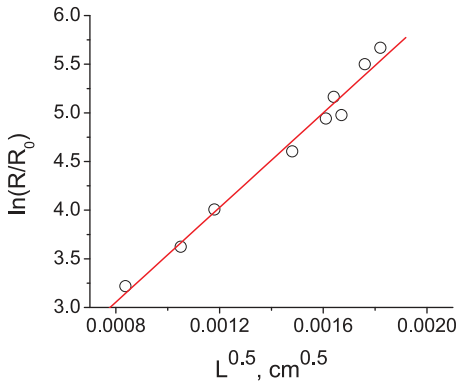

FIG. 19. Logarithm of film resistance R vs. square root of thickness L. Data from Ref. 36 (circles) is fit using the optimum channel field emission mechanism of Eq. (23).

case, conduction through crystalline inclusions should be accounted for.

We shall end this section with a comment regarding possible effects of the Coulomb blockade in extremely small structures.[86,87] Coulomb-blockade effects (whereby the Coulomb interaction between electrons can prohibit their transport) occur in systems where both the tunnel resistance between two sites is large ($r \gg \hbar/e^2 \sim 10$ kΩ) and the charging energy, ($u \sim e^2/2C$), where C is the capacitance of the site, of an excess electron is large compared to kT. The individual sites for the system under consideration can be either localized electronic centers underlying hopping transport or small sample electrodes. As a very rough estimate we assume a current of e/τ_0 between two centers in response to the potential difference kT/e. This leads to the resistance $r \sim kT\tau_0/e^2 \sim 1$ MΩ; it can be even much greater, since the transition time in reality is much longer than τ_0. The capacitive energy can be estimated as simply the Coulomb repulsion energy of two electrons at the same center, $U_c \sim 0.1 - 0.3$ eV. In that case, the Coulomb blockade will impose its related activated transport with the energy barrier $\sim U_c$. We note that even for the case of realistically small devices, the capacitive energy can be significant, $u \sim \varepsilon e^2/2L \sim 1$ eV for the device of characteristic dimensions of $L \sim 10$ nm. In all such cases, single electron transport will dominate the observed current. So far, the possibility of such effects was not considered in connection with chalcogenide glasses. On the other hand, the much larger, above 100 nm structures dominated by band transport, will be rather insensitive to the Coulomb blockade effects.

VI. CONCLUSIONS

In conclusion, we have presented an overview of the experimental data and a comparative analysis of different dc transport mechanisms based on the established physics of chalcogenide glasses. Several models are capable of accounting for the various observed exponential field dependencies of the conductivity. Of the mechanisms considered, Poole-Frenkel ionization, field-induced delocalization of tail states, space-charge limited currents, optimum channel hopping in thin films, optimum channel field emission, percolation band conduction, and transport through crystalline inclusions are all candidate explanations, while Schottky emission and classical hopping conduction are very unlikely. For very thin films ($L \sim 10$ nm), strong thickness-dependent conductivity could be manifested by either percolation band conduction or optimum channel hopping via states with atypically small polaron clouds.

We have shown that it is difficult to identify a particular mechanism through the analysis of IV data alone and further studies are required to discriminate between the different mechanisms. The possibility of interplay between them makes the problem even more challenging.

ACKNOWLEDGMENTS

We are grateful to G. Spadini for encouraging this review and for many useful insights. Discussions with S. A. Kostylev are appreciated. We thank M. Mitra for his explanations of PCM measurements. Also, we acknowledge the Intel grant supporting our research on phase change memory.

[1]S. Lai and T. Lowrey, Tech. Dig. -Int. Electron Devices Meet. **2001**, 803.
[2]S. Eilert, M. Leinwander, and G. Crisenza, in *Proceedings of the IEEE International Memory Workshop, IMW 2009, Monterey, CA, 2009* (IEEE, New York, 2009), pp. 1–2.
[3]T. Morikawa, K. Kurotsuchi, M. Kinoshita, N. Matsuzaki, Y. Matsui, Y. Fujisaki, S. Hanzawa, A. Kotabe, M. Terao, H. Moriya, T. Iwasaki, M. Matsuoka, F. Nitta, M. Moniwa, T. Koga, and N. Takaura, Tech. Dig. -Int. Electron Devices Meet. **2007**, 307.
[4]J. Rodgers, J. Maimon, T. Storey, D. Lee, M. Graziano, L. Rockett, and K. Hunt, in *Proceedings of the IEEE Nonvolatile Memory Technology Symposium, 2008 NVMTS*, Pacific Grove, CA, 2008 (IEEE, New York, 2008), p. 1.
[5]A. Fazio, Tech. Dig. -Int. Electron Devices Meet. **2009**, 641; G. Burr, M. Breitwisch, M. Franceschini, D. Garetto, K. Gopalakrishnan, B. Jackson, B. Kurdi, C. Lam, L. A. Lastras, A. Padilla, B. Rajendran, S. Raoux, and R. S. Shenoy, J. Vac. Sci. Technol. B **28**, 223 (2010).
[6]F. Bedeschi, R. Bez, C. Boffino, E. Bonizzoni, E. C. Buda, G. Casagrande, L. Costa, M. Ferraro, R. Gastaldi, O. Khouri, F. Ottogalli, F. Pellizzer, A. Pirovano, C. Resta, G. Torelli, and M. Tosi, IEEE J. Solid-State Circuits **40**, 1557 (2005).
[7]J. H. Oh, J. H. Park, Y. S. Lim, H. S. Lim, Y. T. Oh, J. S. Kim, J. M. Shin, J. H. Park, Y. J. Song, K. C. Ryoo, D. W. Lim, S. S. Park, J. I. Kim, J. H. Kim, J. Yu, F. Yeung, C. W. Jeong, J. H. Kong, D. H. Kang, G. H. Koh, G. T. Jeong, H. S. Jeong, and K. Kim, Tech. Dig. -Int. Electron Devices Meet. **2006**, S2P6.
[8]F. Pellizzer, A. Benvenuti, R. Gleixner, Y. Kim, B. Johnson, M. Magistretti, T. Marangon, A. Pirovano, R. Bez, and G. Atwood, *in Proceedings of the Symposium on VLSI Technology, 2006, Honolulu, HI, 2006* (IEEE, New York, 2006), p. 122.
[9]G. Servalli, Tech. Dig. -Int. Electron Devices Meet. **2009**, 113.
[10]D. C. Kau, S. Tang, I. V. Karpov, R. Dodge, B. Klehn, J. Kalb, J. Strand, A. Diaz, N. Leung, J. Wu, S. Lee, T. Langtry, K. Chang, C. Papagianni, J. Lee, J. Hirst, S. Erra, E. Flores, N. Righos, H. Castro, and G. Spadini, Tech. Dig. -Int. Electron Devices Meet. **2009**, 617.
[11]I. V. Karpov, D. Kencke, D. Kau, S. Tang, and G. Spadini, in *Proceedings of the Materials Research Society Symposium, San Francisco, CA, 2010* (MRS, Warrendale, PA, 2010), Vol. 1250, G14-01-H07-01.
[12]N. F. Mott and E. A. Davis, *Electronic Processes in Non-crystalline Materials* (Clarendon, Oxford, 1979).
[13]R. M. Hill, Philos. Mag. **23**, 59 (1971).
[14]J. Frenkel, Phys. Rev. **54**, 657 (1938).
[15]H. H. Poole, London, Edinburgh Dublin Philos. Mag. **33**, 112 (1916); H. H. Poole, *ibid*. **34**, 195 (1917).
[16]F. Bedeschi, R. Fackenthal, C. Resta, E. M. Donze, M. Jagasivamani, E. C. Buda, F. Pellizzer, D. W. Chow, A. Cabrini, G. Calvi, R. Faravelli, A. Fantini, G. Torelli, D. Mills, R. Gastaldi, and G. Casagrande, IEEE J. Solid-State Circuits **44**, 217 (2009).
[17]T. Gotoh, J. Non-Cryst. Solids **353**, 2728 (2008).
[18]V. K. Saraswat, V. Kishore, Deepika, N. S. Saxena, T. P. Sharma, L. I. Singh, and P. K. Saraswat, Chalcogenide Lett. **5**, 95 (2008).
[19]M. M. El-Samanoudy, Appl. Surf. Sci. **207**, 219 (2003).
[20]E. A. Lebedev, S. A. Kozykhin, N. N. Konstantinova, and L. P. Kazakova, Semiconductors **43**, 1343 (2009).
[21]N. A. Bogoslowsky and K. D. Tsendin, Semiconductors **43**, 1338 (2009).
[22]E. N. Voronkov and S. A. Kozyukhin, Semiconductors **43**, 921 (2009).
[23]Y. H. Shih, M. H. Lee, M. Breitwisch, R. Cheek, J. Y. Wu, B. Rajendran, Y. Zhu, E. K. Lai, C. F. Chen, H. Y. Cheng, A. Schrott, E. Joseph, R. Dasaka, S. Raoux, H. L. Lung, and C. Lam, Tech. Dig. -Int. Electron Devices Meet. **2009**, 753.
[24]D. Ielmeni and Y. Zhang, J. Appl. Phys. **102**, 054517 (2007); D. Ielmeni and Y. Zhang, Appl. Phys. Lett. **90**, 192102 (2007); D. Ielmini, Phys. Rev. B **78**, 035308 (2008).
[25]D. Allsopp and M. J. Thompson, J. Phys. D: Appl. Phys. **9**, 2075 (1976).
[26]E. A. Lebedev and N. A. Rogachev, Sov. Phys. Semicond. **15**, 86 (1981).
[27]M. P. Shaw, S. H. Holmberg, and S. A. Kostylev, Phys. Rev. Lett. **31**, 542 (1973).
[28]I. F. Kodgespirova, V. A. Shkut, and S. A. Kostylev, in *Proceedings of the International Conference on Amorphous Semiconductors, Bucharest, 1982*, edited by M. Popesku (Springer, 1982), pp. 247–249 (in Russian).

[29]S. D. Savransky and I. V. Karpov, in *Phase-Change Materials for Reconfigurable Electronics and Memory Applications*, edited by A. H. Edwards, P. J. Fons, S. Raoux, P. C. Taylor, and M. Wuttig (Mater. Res. Soc. Symp. Proc., Warrendale, PA, 2008), Vol. 1072E, 1072-G06-09.
[30]J. J. Hauser and R. S. Hutton, Phys. Rev. Lett. **37**, 868 (1976).
[31]A. E. Owen and J. M. Robertson, IEEE Trans. Electron Devices **ED20**, 105 (1973).
[32]P. J. Walsh, R. Vogel, and E. J. Evans, Phys. Rev. **178**, 1274 (1969).
[33]J. M. Robertson, Ph.D. dissertation, University of Edinburgh, 1971.
[34]H. J. de Wit and C. Crevecoeur, J. Non-Cryst. Solids **10**, 787 (1972).
[35]F. Pellizzer, A. Pirovano, F. Ottogalli, M. Magistretti, M. Scaravaggi, P. Zuliani, M. Tosi, A. Benvenuti, P. Besana, S. Cadeo, T. Marangon, R. Moranti, R. Piva, A. Spandre, R. Zonca, A. Modelli, E. Varesi, T. Lowrey, A. Lacaita, G. Casagrande, and R. Bez, in *Proceedings of the Symposium on VLSI Technology, 2004* (IEEE, New York, 2004), p. 1819.
[36]D. Fugazza, D. Ielmini, S. Lavizzari, and A. L. Lacaita, Tech. Dig. -Int. Electron Devices Meet. **2009**, 1; D. Ielmini, D. Fugazza, and M. Boniardi, *Proceedings of the Materials Research Society Symposium, San Francisco, CA, 2011* (MRS, Warrenville, PA, 2011), Vol. 1338, mrss11-1338-r01-04.
[37]A. Calderoni, M. Ferro, D. Ielmini, and P. Fantini, IEEE Electron Device Lett. **31**, 1023 (2010).
[38]P. W. Anderson, Phys. Rev. **109**, 1492 (1958).
[39]P. W. Anderson, Phys. Rev. Lett. **34**, 953 (1975).
[40]S. D. Baranovskii and V. G. Karpov, Fiz. Tech. Poluprovodn. **21**, 3 (1987) [Sov. Phys. Semicond. **21**, 1 (1987)].
[41]S. D. Baranovskii and V. G. Karpov, Fiz. Tech. Poluprovodn. **21**, 314 (1987) [Sov. Phys. Semicond. **21**, 189 (1987)].
[42]R. A. Street and N. F. Mott. Phys. Rev. Lett. **35**, 1293 (1975).
[43]M. Kastner, D. Adler, and H. Fritzsche, Phys. Rev. Lett. **37**, 1504 (1976); M. Kastner and H. Fritzsche, Philos. Mag. **37**, 199 (1978).
[44]B. Huang and J. Robertson, Phys. Rev. B **85**, 125305 (2012).
[45]M. I. Klinger and V. G. Karpov, Zh. Eksp. Teor. Fiz. **82**, 1687 (1982) [Sov. Phys. JETP **55**, 976 (1982)]; V. G. Karpov, *ibid.* **85**, 1017 (1983) [Sov. Phys. JETP **58**, 592 (1983)].
[46]V. G. Karpov, M. I. Klinger, and F. N. Ignatiev, Zh. Eksp. Teor. Fiz. **84**, 761 (1983) [Sov. Phys. JETP **57**, 439 (1983)].
[47]Yu. M. Galperin, V. G. Karpov, and V. I. Kozub, Adv. Phys. **38**, 669 (1989).
[48]D. A. Parshin, Sov. Phys. Solid State **36**, 991 (1994); D. A. Parshin, Phys. Scr., T **49A**, 180 (1993); D. A. Parshin, H. R. Schober, and V. L. Gurevich, Phys. Rev. B **76**, 064206 (2007); B. Ruffle, D. A. Parshin, E. Courtens, and R. Vacher, Phys. Rev. Lett. **100**, 015501 (2008).
[49]W. A. Phillips, Philos. Mag. **34**, 983 (1976).
[50]A. S. Alexandrov and J. T. Devreese, *Advances in Polaron Physics, Series in Solid-State Sciences* (Springer-Verlag, Berlin, 2010).
[51]Yu. A. Firsov, in *Polarons in Advanced Materials*, edited by A. S. Alexandrov, Springer Series in Materials Science (Springer, The Netherlands, 2006), p. 63.
[52]Y. Toyozawa, in *Polarons and Excitons*, edited by C. G. Kuper and G. D. Whitfield (Plenum, New York, 1962), p. 211.
[53]V. G. Karpov, Fiz. Tekh. Poluprovodn. **19**, 123 (1984) [Sov. Phys. Semicond. **19**, 74 (1984)].
[54]A. R. Long. Adv. Phys. **31**, 553 (1982).
[55]S. R. Elliott, Philos. Mag. **36**, 1291 (1977); Philos. Mag. B **40**, 507 (1979).
[56]M. Nardone, V. I. Kozub, I. V. Karpov, and V. G. Karpov, Phys. Rev. B **79**, 165206 (2009).
[57]V. Abakumov, V. Perel, and I. Yassievich, *Nonradiative Recombination in Semiconductors*, Modern Problems in Condensed Matter Science (North-Holland, Amsterdam, 1991), Vol. 33.
[58]S. Lee, D. S. Jeong, J. Jeong, W. Zhe, Y.-W. Park, H.-W. Ahn, and B. Cheong, Appl. Phys. Lett. **96**, 023501 (2010).
[59]B. I. Shklovskii and A. L. Efros, *Electronic Properties of Doped Semiconductors* (Springer-Verlag, New York, 1992).
[60]V. I. Koldyaev, Philos. Mag. B **79**, 331 (1999).
[61]F. Buscemi, E. Piccinini, R. Brunetti, M. Rudan, and C. Jacoboni, J. Appl. Phys. **106**, 103706 (2009).
[62]B.-S. Lee, J. R. Abelsona, S. G. Bishop, D.-H. Kang, B. Cheong, and K.-B. Kim, J. Appl. Phys. **97**, 093509 (2005); M. Frumar, T. Wagner, M. Hrdlicka, B. Frumarovaa, and P. Nemec, E/PCOS (2005).
[63]R. G. D. Jeyasingh, D. Kuzum, and H.-S. P. Wong, IEEE Trans. Electron Devices **58**, 4370 (2011).
[64]S. M. Sze, *Physics of Semiconductor Devices* (Wiley, New York, 1981).
[65]I. M. Lifshits, S. A. Gredeskul, and L. A. Pastur, *Introduction to the Theory of Disordered Systems* (Wiley, New York, 1988).
[66]S. R. Elliott, J. Non-Cryst. Solids **97**, 159 (1987).
[67]M. A. Lampert and P. Mark, *Current Injection in Solids* (Academic, New York, 1970).
[68]I. V. Karpov "Bias dependent Hooge parameter in chalcogenide phase change memory" (unpublished).
[69]T. G. M. Kleinpenning, Physica B+C **94**, 141 (1978).
[70]J. M. Marshall and A. E. Owen, Philos. Mag. **31**, 1341 (1975).
[71]D. Emin, C. H. Seager, and R. K. Quinn, Phys. Rev. Lett. Vol. 28, 813 (1972).
[72]M. L. Knotek, Solid State Commun. **17**, 1431 (1975).
[73]B. Bagley, Solid State Commun. **8**, 345 (1970).
[74]S. D. Baranovskii and V. G. Karpov, Fiz. Tekh. Poluprovodn. **20**, 1811 (1986) [Sov. Phys. Semicond. **20**, 1137 (1986)].
[75]I. V. Karpov and M. Mitra "Temperature dependence of conductivity in a GST based structure" (unpublished).
[76]L. Xu, L. Tong, L. Geng, F. Yang, J. Xu, W. Su, D. Liu, Z. Ma, and K. Chen, J. Appl. Phys. **110**, 013703 (2011).
[77]M. E. Raikh and I. M. Ruzin, in *Mesoscopic Phenomena in Solids*, edited by B. L. Altshuller, P. A. Lee, and R. A. Webb (Elsevier, New York, 1991), p. 315.
[78]E. I. Levin, I. M. Ruzin, and B. I. Shklovskii, Sov. Phys. Semicond. **22**, 401 (1998).
[79]M. Pollak and J. J. Hauser, Phys. Rev. Lett. **31**, 21 (1973).
[80]H. Fritzsche, J. Phys. Chem. Solids **68**, 878 (2007).
[81]Ch. Bapanayyaa, R. Guptaab, and S. C. Agarwal, Philos. Mag. Lett. **91**, 134 (2011).
[82]B. I. Shklovskii, Sov. Phys. Semicond. **13**, 53 (1979).
[83]J. González-Hernández, E. F. Prokhorov, Yu. V. Vorobiev, E. Morales-Sánchez, A. Mendoza-Galván, S. A. Kostylev, Yu. I. Gorobets, V. N. Zakharchecnko, and R. V. Zakarchenko, J. Vac. Sci. Technol. A **19**, 1623 (2001); E. Morales-Sánchez, J. González-Hernández, and E. F. Prokhorov, J. Optoelectron. Adv. Mater. **3**, 333 (2001).
[84]M. Nardone, V. G. Karpov, D. C. S. Jackson, and I. V. Karpov, Appl. Phys. Lett. **94**, 103509 (2009).
[85]S. A. Kostylev, in *Proceedings of the Non-Volatile Memory Symposium*, Portland, OR, 2009 (IEEE, New York, 2009), pp. 16–23.
[86]D. V. Averin and K. K. Likharev, in *Mesoscopic Phenomena in Solids*, edited by B. L. Altshuler, P. A. Lee, and R. A. Webb (Elsevier, Amsterdam, 1991).
[87]*Single Charge Tunneling: Coulomb Blockade Phenomena in Nanostructures*, edited by H. Grabert and M. H. Devoret (Plenum, New York, 1992).